Supplementary Information

Development of an integrated polyoxoniobate catalyst with oxygen activation and basicity as a green catalyst for efficient aerobic oxidation of aldehydes at room temperature

Yan-Ru Li, Chun-Xia Chen, Ke-Xin Qi, Cai Sun* and Shou-Tian Zheng*

[a]Fujian Provincial Key Laboratory of Advanced Inorganic Oxygenated Materials, College of Chemistry, Fuzhou University, Fuzhou, Fujian, 350108, China

E–mails: csun@fzu.edu.cn (C. Sun); stzheng@fzu.edu.cn (S.-T. Zheng)

Table of Contents

1. General Information

The Fourier transform infrared (FT-IR) spectra were recorded in the 400-4000 cm^{-1} spectral region using a Nicolet IS50 spectrometer. Phase identification was performed through powder X-ray diffraction (PXRD) measurements on a Rigaku MiniFlex 600 system with Cu Kα radiation (λ = 1.54056 Å), scanning across the 2θ range of 5-50°. Thermal stability was evaluated via thermogravimetric analysis (TGA) using a Mettler Toledo TGA/SDTA 851^e thermal analyzer under ambient atmosphere, with temperature ramping from 30 °C to 800 °C at 10 °C/min. Morphological characterization and elemental distribution mapping were achieved using a Zeiss Sigma 300 field-emission scanning electron microscope (FE-SEM) equipped with energy-dispersive X-ray spectroscopy (EDS). The gas adsorption properties (N_2) and specific surface area of Co-Ti_2Nb_8 were evaluated using a Micromeritics ASAP 2020 accelerated surface area and porosimetry analyzer. Temperature control was achieved through cryogenic bath: 77 K using liquid nitrogen. ^{1}H (400 MHz) and ^{13}C (100 MHz) NMR spectra were recorded using a JEOL ECZ400 (400 MHz) spectrometer and Bruker AV-400 (400 MHz). Proton chemical shifts are reported relative to the residual solvent peak (DMSO at 2.50 ppm). Carbon chemical shifts are reported relative to DMSO at 39.5 ppm. Date are represented as follows: chemical shift, multiplicity (br = broad, s = singlet, d = double, t = triplet, q = quartet, m = multiplet), coupling constants in Hertz (Hz), integration. Mass spectra were recorded on a SHIMADZU GCMS-QP2050 equipped with an SH-I-5Sil MS Cap Column (30m, 0.25mm ID, 0.25μm). H_2O was deionized. Other reagents were purchased from commercial sources and used without further purification.

2. Synthesis of Catalysts and Starting Materials

Synthesis of $[Co(en)_3]_3$ $[Ti_2Nb_8O_{28}]$ $(OH)\cdot 11H_2O$ (Co-Ti_2Nb_8)

The compound Co-Ti_2Nb_8 was synthesized based on the literature method.[1] A mixture of $K_7H[Nb_6O_{19}]\cdot 13H_2O$ (0.666 g, 0.486 mmol), $Co(Ac)_2\cdot 4H_2O$ (0.150 g, 0.612 mmol), K_2TiF_6 (0.156 g, 0.650 mmol), $Li_2B_4O_7$ (0.063 g, 0.371 mmol) and $NaHCO_3$ (0.176 g, 2.09 mmol) was added into 8.0 mL distilled water. In addition, 0.10 mL en (en = ethylenediamine) were added into the solution, stirred for 1 hour, and then transferred to a 20 mL glass bottle. It was kept at 100 °C for 3 days, and cooled to room temperature. The long yellow strip crystals Co-Ti_2Nb_8 were obtained by further washing with distilled water and then air-dried.

Synthesis of $[Cu(en)_2][Cu(en)_2(H_2O)_2]_3[TiNb_8O_{28}]\cdot 8H_2O$ (Cu-Ti_2Nb_8)

The compound $Cu_4Ti_2Nb_8$ was synthesized based on the literature method.[2] $K_7H[Nb_6O_{19}]\cdot 13H_2O$ (0.100 g, 0.073 mmol), $Cu(NO_3)_2\cdot 3H_2O$ (0.100 g, 0.414 mmol), titanium isopropoxide (0.300 mL, 0.989 mmol) were mixed in 8.0 mL H_2O. Then 0.25 mL en were added to the mixture. The mixture was transferred into a 23 mL capacity PTFE-lined autoclave and heated at 140 °C for 3 days. After cooling to room temperature, purple block-like crystals were obtained, washed with distilled water, and then air-dried.

Synthesis of $Na_8[Ti_2Nb_8O_{28}]\cdot 34H_2O$ (Na-Ti_2Nb_8)

The compound Na-Ti_2Nb_8 was synthesized based on the literature method.[3] Amorphous niobium pentoxide (0.350 g, 1.316 mmol) and titanium isopropoxide (0.267 g, 0.880 mmol) are combined in an 8 mL NaOH solution (0.34 M) in a 23 mL Teflon-lined Parr pressure vessel and stirred for approximately 20 min. The closed vessel is placed in an oven at 200–220°C for 5–20 h. The product is a mixture of white powder and irregular-shaped, colorless crystals that dehydrate quickly (become cracked and translucent) when removed from the mother liquor. To obtain a pure batch of crystals, the product mixture is stirred in de-ionized water. The crystals dissolve and the white powder is filtered off. A clear solution is obtained from this treatment that contains the dissolved crystals. Slow diffusion of methanol into the solution at room temperature produces well-formed crystals.

Synthesis of $Co(en)_3ClSO_4$

The compound $Co(en)_3ClSO_4$ was synthesized based on the literature method.[4] In a 200 mL beaker, sequentially add of concentrated en (2.300 mL, 16.547 mmol), concentrated HCl (2.500 mL, 29.750 mmol) and an $CoSO_4\cdot 7H_2O$ aqueous solution (0.538 M). Add 0.500 g activated carbon and stir the mixture vigorously. Then, gradually add H_2O_2 to the system until the solution turns orange-red, indicating that all divalent cobalt has been oxidized. Adjust the pH to 7.0 by adding HCl. Heat the mixture for 15 minutes. After heating, cool the mixture and filter to collect the solid. Allow the filtrate to stand for 2 days, during which orange-yellow crystals will form and can be extracted.

Synthesis of $H_2[Co(en)_3]_2(Nb_6O_{19})\cdot 9H_2O$ (Co-Nb_6)

A mixture of $K_7H[Nb_6O_{19}]\cdot 13H_2O$ (0.319 g, 0.233 mmol), $CoCl_2\cdot 6H_2O$ (0.080 g, 0.336 mmol) was added into 8.0 mL distilled water. In addition, 0.2 mL en were added into the solution, stirred for 1 hour, and then transferred to a 20 mL glass bottle. It was kept at 80 °C for 3 days, and cooled to room temperature. The yellow square crystals were obtained by further washing with distilled water and air-dried.

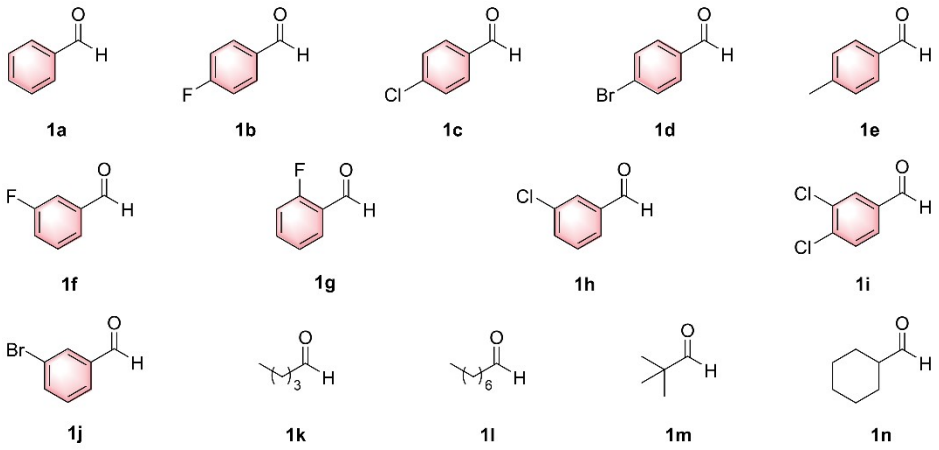

Figure S1. Reaction scope of aldehydes

3. Optimization of Reaction Conditions

Procedure A: To a 25 mL Schlenk tube, **1a**, Co-Ti_2Nb_8 (0.5 mol%, 0.005 mmol), and solvent (2.0 mL) were added under 1 atm O_2 atmosphere. The mixture was stirred at r.t. for 1 h. After the reaction mixture was tested by GC.

Table S1. Screening of solvents

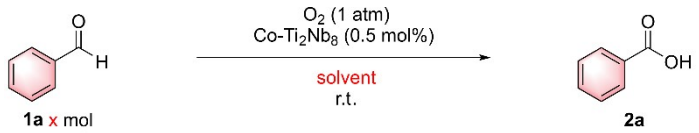

Entry	Solvent	BzH/mmol	Yield (%)
1	Toluene	1	26
2	EtOH	1	<5
3	DCM	1	43
4	Acetone	1	23
5	H_2O/MeCN (3:1)	1	27
6	H_2O/MeCN (1:3)	1	74
7	H_2O/Toluene	1	<5
8	H_2O/EtOH	1	<5
9	H_2O/MeCN	0.5	97
10	H_2O/MeCN	1	>99
11	H_2O/MeCN	1.5	92
12	H_2O/MeCN	2	82

4. The Scope of Aldehydes

Procedure B: To a 25 mL Schlenk tube, **1** (1.00 mmol), Co-Ti_2Nb_8 (0.5 mol%, 0.005 mmol) and H_2O/ MeCN (2.0 mL) were added under 1 atm O_2 atmosphere. The mixture was stirred at rt for 1 h. Then, the reaction mixture was added 40 mg of NaOH (1.00 mmol) and stir for 5 minutes. Next, followed by 3 ml of DCM to wash the aqueous phase, repeating this step three times. Adjust the pH of the aqueous phase to 2 using 0.1 M HCl, and then wash with 5 ml of ether, again repeating this step three times. Collect the ether (a total of 15 ml) and add anhydrous sodium sulfate to remove any residual water, shaking the mixture and allowing it to stand for 20 minutes. Finally, filter out the anhydrous sodium sulfate solid and rotary evaporate the collected filtrate to obtain the product. The crude mixture also can be purified by column chromatography on silica gel.

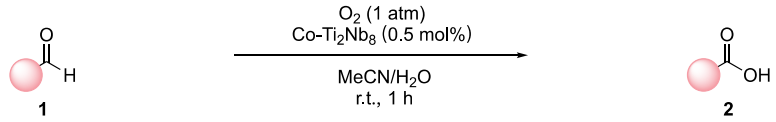

Synthesis of compound 2a

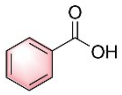

Benzoic acid (**2a**), white crystal, 121.93 mg, 99%.

^{1}H NMR (400 MHz, DMSO) δ 7.48 (t, *J* = 7.6 Hz, 2H), 7.59 (t, *J* = 7.6 Hz, 1H), 7.95 (d, *J* = 7.6 Hz, 2H), (COOH is missing).

^{13}C NMR (100 MHz, DMSO) δ 128.7 (2C), 129.4 (2C), 130.9, 133.0, 167.6.

Synthesis of compound 2b

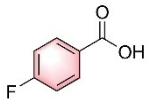

p-Fluorobenzoic acid (**2b**), white powder, 138.7 mg, 99%.

^{1}H NMR (400 MHz, DMSO) δ 7.28–7.34 (m, 2H), 7.97–8.02 (m, 2H), 13.05 (br, 1H).

^{13}C NMR (100 MHz, DMSO) δ 115.6, 115.8, 127.4, 132.16, 132.25, 163.8, 166.3, 166.5.

Synthesis of compound 2c

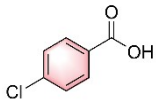

p-Chlorobenzoic acid (**2c**), white powder, 150.31 mg, 96%.

^{1}H NMR (400 MHz, DMSO) δ 7.54 (d, *J* = 8.4 Hz, 2H), 7.93 (d, *J* = 8.4 Hz, 2H), 13.18 (br, 1H).

^{13}C NMR (100 MHz, DMSO) δ 128.7 (2C), 129.7, 131.2 (2C), 137.8, 166.5.

Synthesis of compound 2d

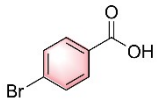

p-Bromobenzoic acid (**2d**), white powder, 180.93 mg, 90%.

^{1}H NMR (400 MHz, DMSO) δ 7.70 (d, *J* = 8.0 Hz, 2H), 7.86 (d, *J* = 8.0 Hz, 2H), 13.20 (br, 1H).

^{13}C NMR (100 MHz, DMSO) δ 127.0, 130.0, 131.4 (2C), 131.8 (2C), 166.7.

Synthesis of compound 2e

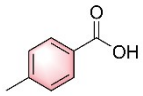

p-methylbenzoic acid (**2e**) (for 4 h), white powder, 134.81 mg, 99%.

^{1}H NMR (400 MHz, DMSO) δ 2.34 (s, 3H), 7.27 (d, *J* = 8.0 Hz, 2H), 7.84 (d, *J* = 8.0 Hz, 2H), 12.82 (br, 1H).

^{13}C NMR (100 MHz, DMSO) δ 21.2, 128.1, 129.2 (2C), 129.4 (2C), 143.1, 167.5.

Synthesis of compound 2f

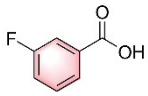

m-Fluorobenzoic acid (**2f**) (for 4 h), white powder, 125.13 mg, 90%.

^{1}H NMR (400 MHz, DMSO) δ 7.44–7.93 (m, 1H), 7.52–7.58 (m, 1H), 7.63–7.66 (m, 1H), 7.77–7.79 (m, 1H), 13.26 (br, 1H).

^{13}C NMR (100 MHz, DMSO) δ 115.7, 115.9, 119.8, 120.0, 125.49, 125.52, 130.8, 130.9, 133.26, 133.33, 160.8, 163.3, 166.27, 166.30.

Synthesis of compound 2g

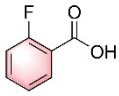

o-Fluorobenzoic acid (**2g**) (for 12 h), white powder, 90.38 mg, 65%.

^{1}H NMR (400 MHz, DMSO) δ 7.28 (t, *J* = 8.4 Hz, 2H), 7.61 (q, *J* = 7.2 Hz, 1H), 7.87 (t, *J* = 7.6 Hz, 1H), 13.25 (br, 1H).

^{13}C NMR (100 MHz, DMSO) δ 116.8, 117.1, 119.2, 119.5, 134.45, 124.49, 132.0, 134.7, 134.8, 159.9, 162.5, 165.12, 165.15.

Synthesis of compound 2h

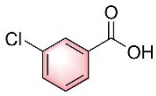

3-Chlorobenzoic acid (**2h**) (for 4 h), white powder, 128.37 mg, 82%.

^{1}H NMR (400 MHz, DMSO) δ 7.53 (t, *J* = 8.0 Hz, 1H), 1.54–1.59 (ddd, *J* = 8.0, 2.0, 1.2 Hz, 1H), 7.88–7.90 (m, 2H), 13.35 (s, 1H).

^{13}C NMR (100 MHz, DMSO) δ 128.0, 128.9, 130.7, 132.8, 133.4, 166.1.

Synthesis of compound 2i

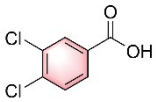

3,4-Dichlorobenzoic acid (**2i**), white powder, 160.37 mg, 84%.

^{1}H NMR (400 MHz, DMSO) δ 7.75 (d, *J* = 8.4 Hz, 1H), 7.87 (dd, *J* = 8.4, 2.0 Hz, 1H), 8.04 (d, *J* = 2.0 Hz, 1H), (COOH is missing).

^{13}C NMR (100 MHz, DMSO) δ 129.4, 131.0, 131.1, 131.5, 131.6, 135.9, 165.5.

Synthesis of compound 2j

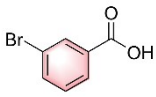

m-Bromobenzoic acid (**2j**) (for 4h), white powder, 178.90 mg, 89%.

^{1}H NMR (400 MHz, DMSO) δ 7.43 (t, *J* = 8.0, 1H), 7.76 (d, *J* = 8.0, 1H), 7.90 (d, *J* = 8.0, 1H), 8.00 (s, 1H), (COOH is missing).

^{13}C NMR (100 MHz, DMSO) δ 122.0, 128.5, 131.0, 132.0, 133.3, 135.8, 166.3.

Synthesis of compound 2k

Valeric acid (**2i**), colorless oil, 101.09 mg, 99%

^{1}H NMR (400 MHz, DMSO) δ 0.81 (t, *J* = 7.2 Hz, 3H), 1.23 (h, *J* = 7.6 Hz, 2H), 1.43 (p, *J* = 7.6 Hz, 2H), 2.13 (t, *J* = 7.2 Hz, 2H), (COOH is missing).

^{13}C NMR (100 MHz, DMSO) δ 14.2, 22.5, 27.4, 34.2, 175.6.

Synthesis of compound 2l

Octanoic acid (**2l**), colorless oil, 144.13 mg, 99%.

^{1}H NMR (400 MHz, DMSO) δ 0.85 (t, *J* = 7.2 Hz, 3H), 1.20–1.28 (m, 8H), 1.48 (p, *J* = 7.2 Hz, 2H), 2.17 (t, *J* = 7.2 Hz, 2H), 11.96 (s, 1H),

^{13}C NMR (100 MHz, DMSO) δ 13.9, 22.1, 24.6, 28.5, 28.6, 31.3, 33.7, 174.5.

Synthesis of compound 2m

Pivalic acid (**2m**), colorless oil, 101.12 mg, 99%.

^{1}H NMR (400 MHz, DMSO) δ 1.10 (s, 9H).

^{13}C NMR (100 MHz, DMSO) δ 27.1, 37.8, 179.5.

Synthesis of compound 2n

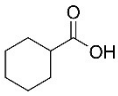

Cyclohexanecarboxylic acid (**2n**), colorless oil, 126.90 mg, 99%.

^{1}H NMR (400 MHz, DMSO) δ 1.14–1.36 (m, 5H), 1.54–1.59 (m, 1H), 1.62–1.67 (m, 2H),1.77–1.81 (m, 2H), 2.14–2.21(m, 1H), 12.00 (s, 1H).

^{13}C NMR (100 MHz, DMSO) δ 25.2 (2C), 25.7, 29.0 (2C), 42.5, 177.0.

5. Gram-scale Reaction

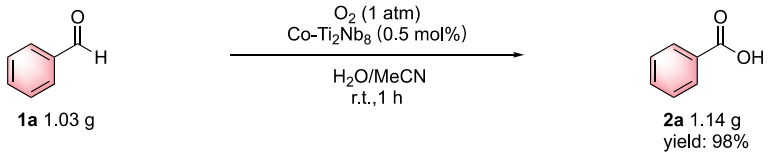

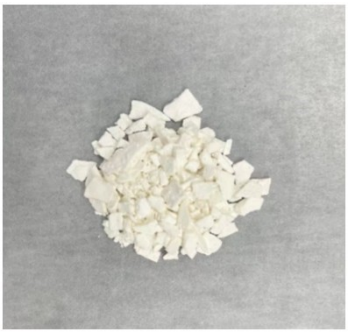

Benzaldehyde (**1a**, 1.03 g, 9.706 mmol), Co-Ti_2Nb_8 (94.34 mg, 0.048 mmol, 0.5 mol%), acetonitrile (9.7 mL) and deionized H_2O (9.7 mL) were added to a 100 mL round-bottomed flask under 1 atm O_2 atmosphere. The mixture was stirred at rt for 1 h. After the reaction, the mixture was filtered to remove catalyst. Then, the reaction mixture was added 400 mg of NaOH (10.00 mmol) and stir for 5 minutes. Next, followed by 20 ml of DCM to wash the aqueous phase, repeating this step three times. Adjust the pH of the aqueous phase to 2 using 0.1 M HCl, and then wash with 30 ml of ether, again repeating this step three times. Collect the ether (a total of 90 ml) and add anhydrous sodium sulfate to remove any residual water, shaking the mixture and allowing it to stand for 1 hour. Finally, filter out the anhydrous sodium sulfate solid and rotary evaporate the collected filtrate to obtain 1.14 g **2a**.

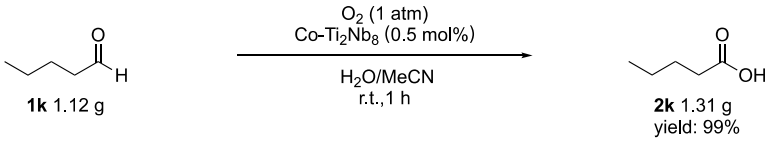

Valeraldehyde (**1k**, 1.12 g, 13.00 mmol), Co-Ti_2Nb_8 (127.75 mg, 0.065 mmol, 0.5 mol%), acetonitrile (13 mL) and deionized H_2O (13 mL) were added to a 100 mL round-bottomed flask under 1 atm O_2 atmosphere. The mixture was stirred at rt for 1 h. Then, using same processing method, 1.13 g **2k** was obtained.

6. Investigation of Reaction Mechanism

6.1. Investigation of active component of Co-Ti_2Nb_8

Table S2. Investigation the effects of different components of catalysts

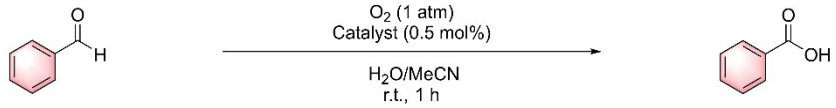

Entry	Catalyst	Yield
1	Co-Ti_2Nb_8	>99
2	$Co(OAc)_2$	58
3	$Co(en)_3ClSO_4$	53
4	Co-Nb_6	>99[a]
5	Cu-Ti_2Nb_8	0
6	Na-Ti_2Nb_8	0
7	Nb_6	0

[a]Reaction time is 6 h. Using 1 mmol benzaldehyde. Nb_6 is $KH_7Nb_6O_{19}$. Solvent is 2.0 mL and the volume of ratio of H_2O and MeCN is 1:1. Yields are calculated by GC.

6.2. Investigating the basicity of different catalysts

Weigh 0.005 mmol of each catalyst and place them into six parallel glass bottles. Add 2 mL of deionized water to each bottle, stir the mixtures under air for 1 hour, and measure the pH using a pH test pen. The experimental results are presented in Table S3. According to the experimental results, the addition of $CoNb_6$ and Co-Ti_2Nb_8 facilitated the dissociation of H_2O, leading to an increase in the pH of the solution. This increase is likely attributed to the binding of hydrolytically separated H^+ by niobium clusters, which act as Brønsted bases.

Table S3. Investigating the basicity of different catalysts

Entry	Catalyst	Solubility	pH
1	Co-Ti_2Nb_8	insoluble	10.2
2	$Co(OAc)_2$	soluble	7.2
3	$Co(en)_3ClSO_4$	soluble	5.2
4	Co-Nb_6	insoluble	9.4
5	Cu-Ti_2Nb_8	insoluble	7.6
6	Na-Ti_2Nb_8	insoluble	9.3
7	Nb_6	soluble	11.1

Catalyst: 0.005 mmol; H_2O: 2 mL (pH = 5.5 dissolution of carbon dioxide); stir for 1 h.

6.3. The roles of lattice waters on the catalysts surface

All experiments were performed under standard conditions, and the corresponding yields were determined by GC. In the absence of lattice water, the Co-Nb_6 catalyst showed minimal reactivity within 6 h, while the reaction yield for Co-Ti_2Nb_8 decreased to 55% for 1 h. Upon extending the reaction time to 12 h, the yield for the Co-Nb_6-catalyzed reaction increased to 95%, whereas the yield for the Co-Ti_2Nb_8-catalyzed reaction reached 99% for 4 h. These results indicate that lattice water on the catalyst surface significantly influences the reaction rate.

Table S4. Investigating the roles of lattice waters on catalysts

Entry	Catalyst	t (h)	Yield
1	Co-Nb_6 (with lattice H_2O)	1	n.r.
2	Co-Nb_6 (with lattice H_2O)	6	>99
3	Co-Nb_6 (no lattice H_2O)	6	n.r.
4	Co-Nb_6 (no lattice H_2O)	12	95
5	Co-Ti_2Nb_8 (with lattice H_2O)	1	>99
6	Co-Ti_2Nb_8 (no lattice H_2O)	1	55
7	Co-Ti_2Nb_8 (no lattice H_2O)	4	>99

Using 1 mmol benzaldehyde. Solvent is 2 mL and the volume of ratio of H_2O and MeCN is 1:1. Yields are calculated by GC. With lattice H_2O (r.t., air drying 2 days), no lattice H_2O (r.t., vacuum drying 15 h), n.r. = no reaction.

6.4. Time-dependent yield changes of the Co-Ti_2Nb_8 and $CoNb_6$ systems

Six parallel reactions were carried out at the different time. To a 25 mL Schlenk tube, **1a**, Co-Ti_2Nb_8 (0.5 mol%, 0.005 mmol), and solvent (2.0 mL) were added under 1 atm O_2 atmosphere. After the reaction mixture was tested by GC. Then six parallel experiments were also performed using Co-Nb_6 as catalyst. The experimental results showed that the induction time for Co-Ti_2Nb_8 was significantly shorter than that for Co-Nb_6. This may be attributed to the presence of hydroxyl groups (OH) bound to the Co in the Co-Ti_2Nb_8 structure, shortening the time of obtaining OH from lattice water.

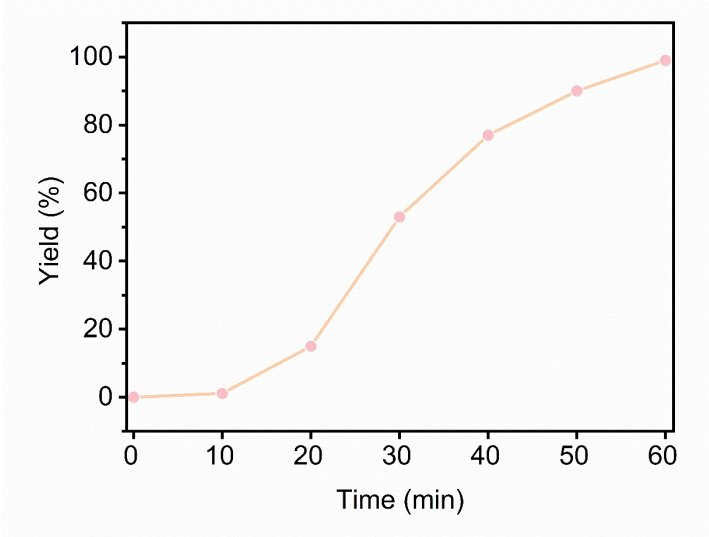

Figure S2. Time-dependent yield changes of the Co-Ti_2Nb_8.

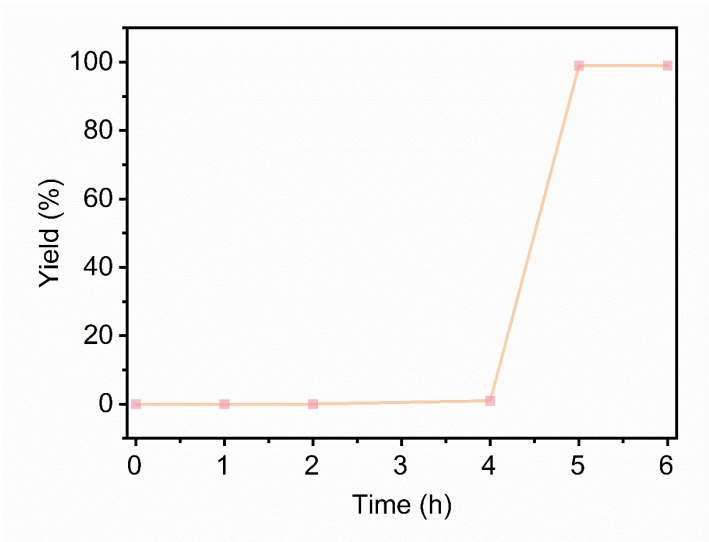

Figure S3. Time-dependent yield changes of the Co-Nb_6.

6.5. Isotope labeling experiment

In two controlled experiments, benzaldehyde (0.25 mmol), Co-Ti_2Nb_8 (0.5 mol%), and acetonitrile (0.25 mL) were added to a Schlenk tube. The difference between the experiments was the solvent used: (a) H_2O and (b) $H_2{}^{18}O$. After 1 hour, the oxidized product **2a** and $H_2{}^{18}O$ labeled **2a** were analyzed by GC-MS.

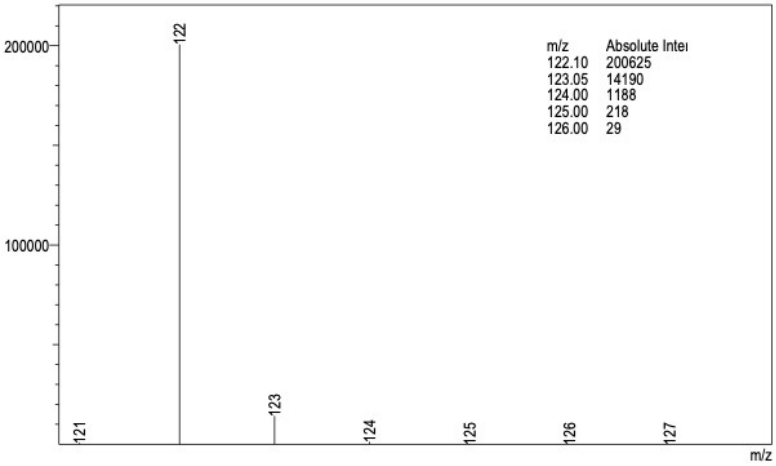

Figure S4. Mass spectrometry data of product that prepared in H_2O/MeCN.

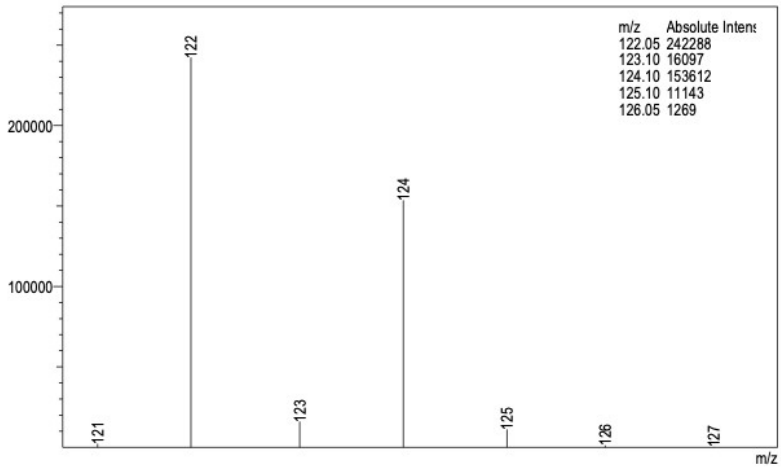

Figure S5. Mass spectrometry data of product that prepared in $H_2{}^{18}O$/MeCN.

Table S5. Calculation of isotopic enrichment relative of product that prepared in $H_2{}^{18}O$/MeCN

m/z	Relative Natural Abundance (%)	Observed Abundance (%)	Corrected Abundance (%)	Isotopic Enrichment Relative (%)
[M]+0	100	242288	242288	61.2
[M]+2	0.59	153612	152183	38.5
[M]+4	0.01	1269	1234	0.30

The ratio of the relative natural abundances of [M]+0, [M]+2, and [M]+4 was calculated based on the results from experiment (a). The observed abundances of [M]+0, [M]+2, and [M]+4 were obtained

from experiment (b). The corrected abundances were calculated using the following formulas:

For [M]+2:

[M]+2 = 153612– (242288*0.59) = 152183

For [M]+4:

[M]+4 = 1269– (242288*0.01) = 1234

7. Characters of Catalysts

Infrared (IR) spectra (KBr pellet) were performed on an Opus Vetex 70 FT-IR infrared spectrophotometer in the range of 400−4000 cm^{-1}. Powder X-ray diffraction (PXRD) patterns were recorded on a Rigaku DMAX 2500 diffractometer with Cu K_α radiation (λ = 1.54056 Å). Simulated PXRD pattern was derived from the Mercury Version 4.3.0 software using the X-ray single crystal diffraction data. Thermogravimetric analyses were conducted using a Mettler Toledo TGA/SDTA 851e analyzer in an N_2-flow atmosphere with a heating rate of 10 °C/min at a temperature of 30−800 °C. X-ray photoelectron spectroscopy (XPS) studies were performed in a ThermoFisher ESCALAB250 X-ray photoelectron spectrometer (powered at 150 W) using Al K_α radiation (λ = 8.357 Å).

Table S6. Crystal and structure refinement data of Co-Ti_2Nb_8 and Cu-Ti_2Nb_8

	Co-Ti_2Nb_8	**Cu-Ti_2Nb_8**
Formula	$C_{18}H_{95}Co_3N_{18}Nb_8O_{40}Ti_2$	$C_{16}H_{92}Cu_4N_{16}Nb_8O_{42}Ti_2$
Mr	2219.98	2347.24
Crystal size (mm^3)	0.3 × 0.1 × 0.1	0.2 × 0.2 × 0.1
Crystal system	monoclinic	triclinic
Space group	$P2_1/c$	$P\text{-}1$
***a* (Å)**	12.1776(4)	11.0384(14)
***b* (Å)**	38.7820(14)	12.372(2)
***c* (Å)**	14.7815(6)	15.223(3)
α (deg)	90	102.841(2)
β (deg)	100.796(4)	109.557(2)
γ (deg)	90	105.849(2)
***V* (Å^3)**	6857.3(4)	1703.8(8)
D_{calcd} (g/cm^3)	2.150	2.288
Z	4	2
***F*(000)**	4396.0	2298.0
Abs coeff (mm^{-1})	2.305	2.840
Refl. Collected	62174	32377
Data/params/restraints	15898/1144/1182	12139/856/12
R_1[a]	0.0830	0.0545
ωR_2[b]	0.1942	0.1707
GOF on F^2	1.089	0.912
$\Delta\rho_{max}$ and $\Delta\rho_{min}$ (e/Å^3)	1.48 and -1.35	2.31 and -1.25

[a]$R_1 = \sum||F_o|-|F_c||/\sum|F_o|$, [b]$\omega R_2 = \{\sum\omega[(F_o)^2-(F_c)^2]^2/\sum\omega[(F_o)_2]^2\}^{1/2}$.

Table S7. Crystal and structure refinement data of Na-Ti_2Nb_8 and Co-Nb_6

	Na-Ti_2Nb_8	**Co-Nb_6**
Formula	$Na_8Ti_2Nb_8O_{62}$	$C_{12}H_{68}Co_2N_{12}Nb_6O_{35}$
Mr	2014.866	1616.10
Crystal size (*mm*^{3})	0.2 × 0.1 × 0.1	0.05 × 0.05 × 0.05
Crystal system	Triclinic	cubic
Space group	*P*-1	*Pn-3m*
***a* (Å)**	11.7788(12)	14.319(3)
***b* (Å)**	12.1971(13)	14.319(3)
***c* (Å)**	12.5491(12)	14.319(3)
α (deg)	97.816(2)	90
β (deg)	113.849(2)	90
γ (deg)	110.778(2)	90
***V* (Å^3)**	1457.1(3)	2935.8(18)
D_{calcd} (g/cm^3)	2.296	1.828
Z	1	2
***F*(000)**	940.9	1608.0
Abs coeff (mm^{-1})	1.956	1.768
Refl. Collected	13823	8520
Data/params/restraints	5036/0/359	567/33/1
R_1[a]	0.0306	0.0600
ωR_2[b]	0.0939	0.1838
GOF on F^2	1.043	1.051
$\Delta\rho_{max}$ and $\Delta\rho_{min}$ (e/Å^3)	2.75 and -2.79	1.38 and -0.49

[a]$R_1 = \sum||F_o|-|F_c||/\sum|F_o|$, [b]$\omega R_2 = \{\sum\omega[(F_o)^2-(F_c)^2]^2/\sum\omega[(F_o)_2]^2\}^{1/2}$.

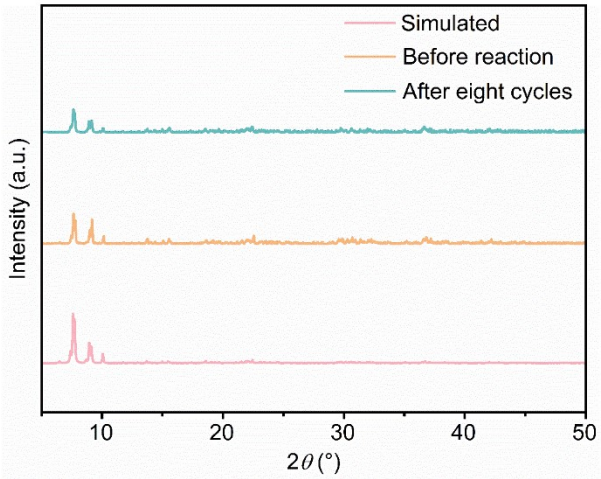

Figure S6. PXRD pattern spectra of Co-Ti_2Nb_8 and after 8 cycles.

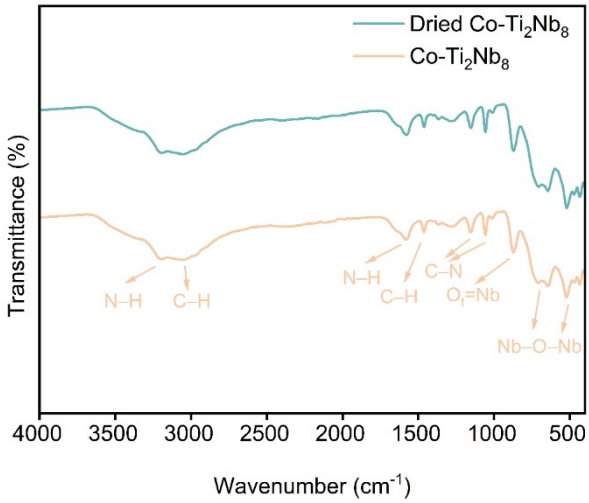

Figure S7. IR spectra of Co-Ti_2Nb_8.

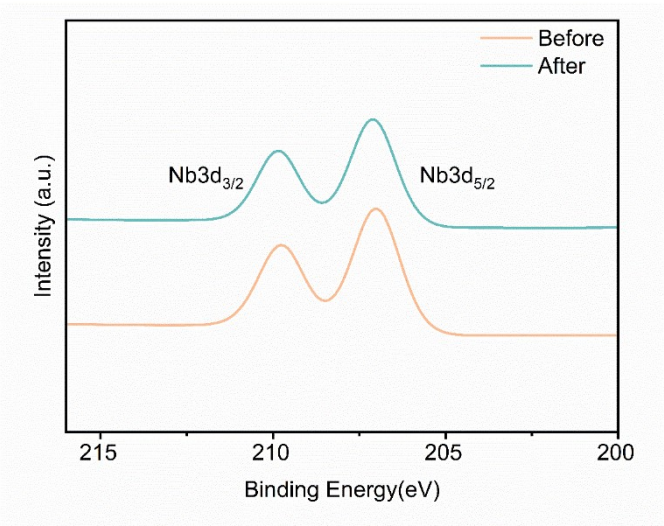

Figure S8. XPS (Al K_α) core-level spectra for Nb 3d of the before and after 8 cycles.

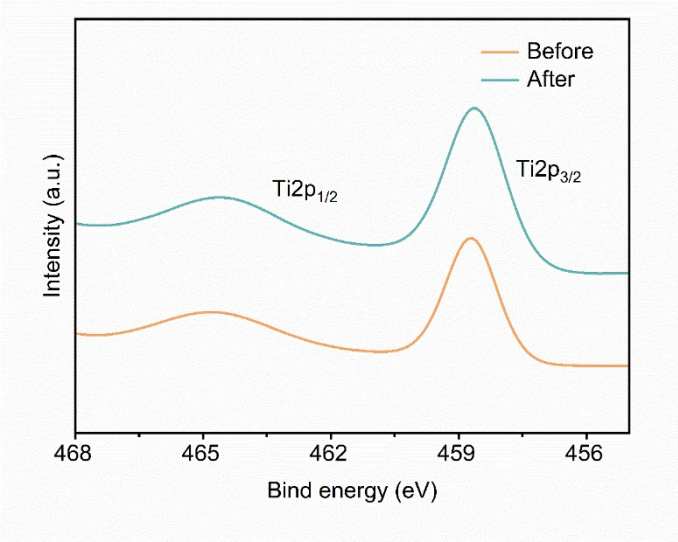

Figure S9. XPS (Al K_α) core-level spectra for Ti 2p of the before and after 8 cycles.

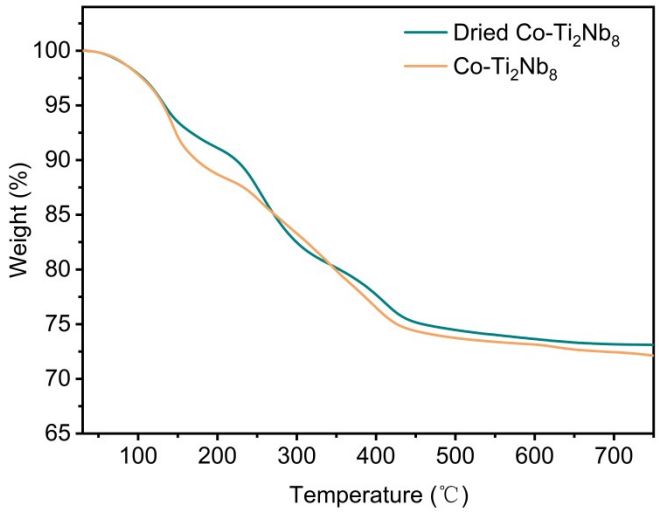

Figure S10. Thermogravimetric analysis of dried Co-Ti_2Nb_8 and Co-Ti_2Nb_8.

Through the thermogravimetric curve of Co-Ti_2Nb_8, it is hypothesized that 11 lattice water molecules in Co-Ti_2Nb_8 crystal.

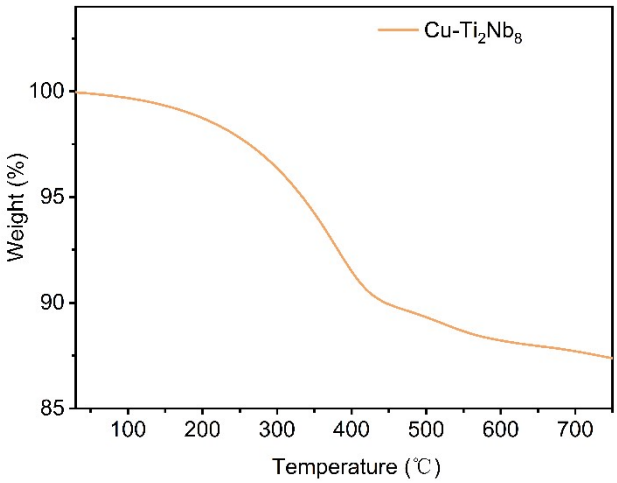

Figure S11. Thermogravimetric analysis of Cu-Ti_2Nb_8

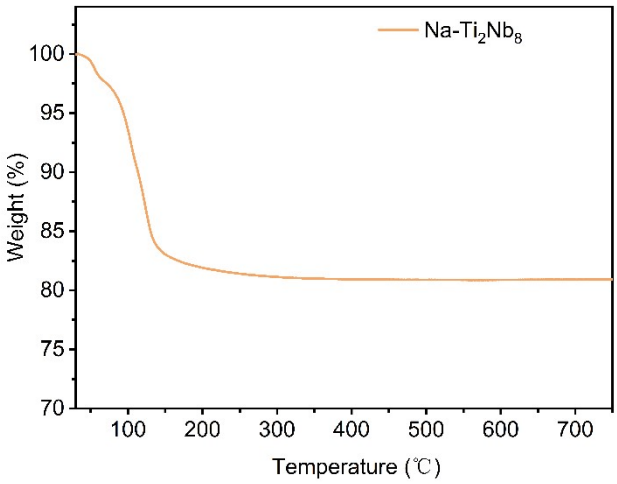

Figure S12. Thermogravimetric analysis of Na-Ti_2Nb_8.

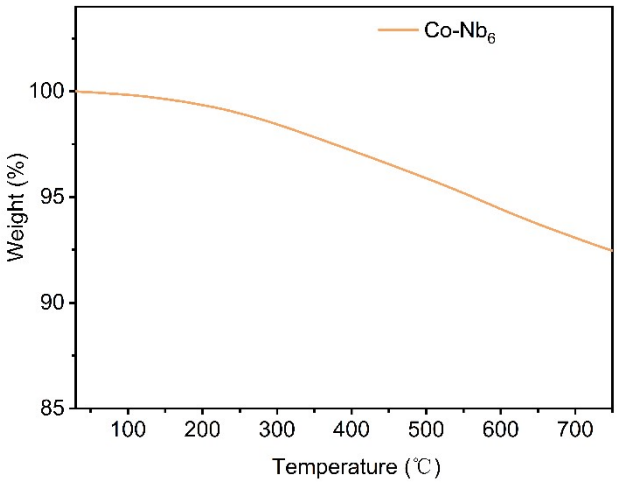

Figure S13. Thermogravimetric analysis of Co- Nb_6.

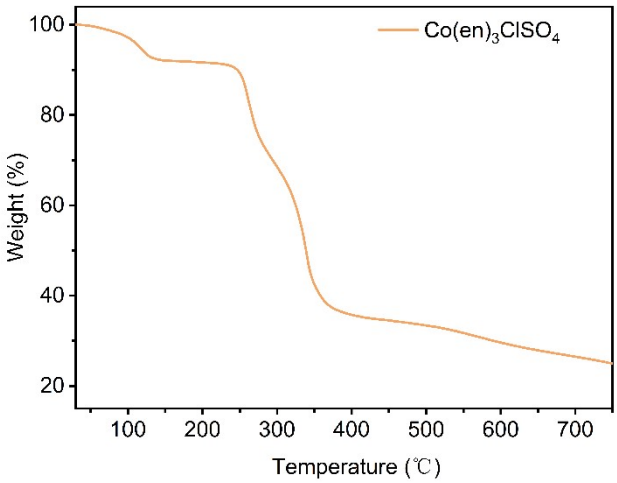

Figure S14. Thermogravimetric analysis of $Co(en)_3ClSO_4$.

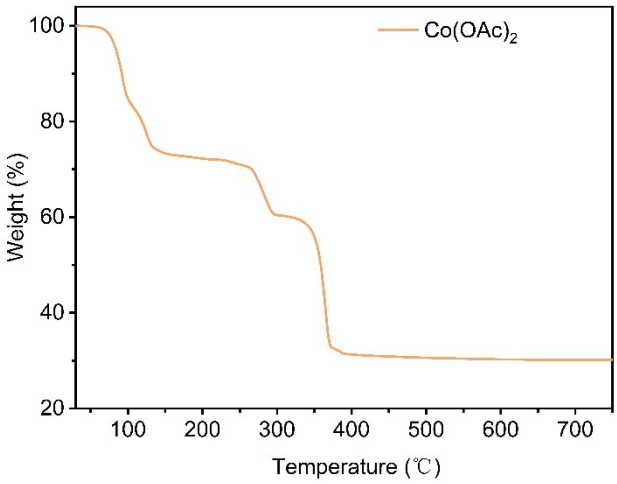

Figure S15. Thermogravimetric analysis of $Co(OAc)_2$.

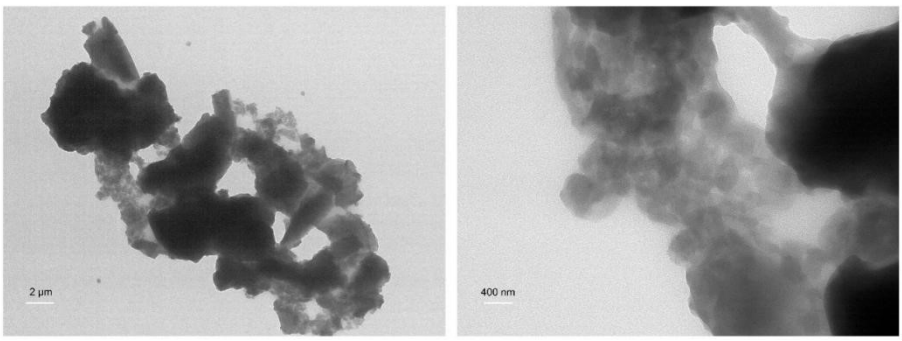

Figure S16. TEM images of Co-Ti_2Nb_8.

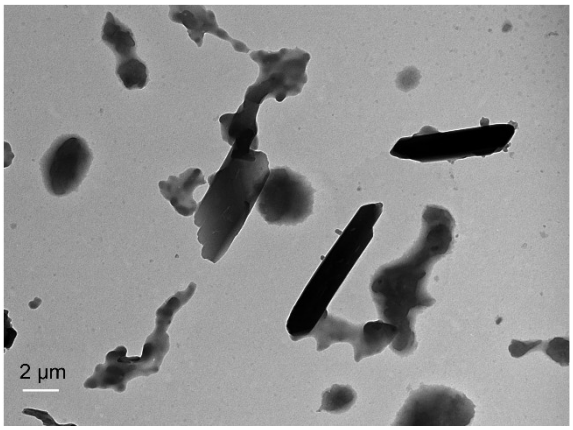

Figure S17. TEM images of Cu-Ti_2Nb_8.

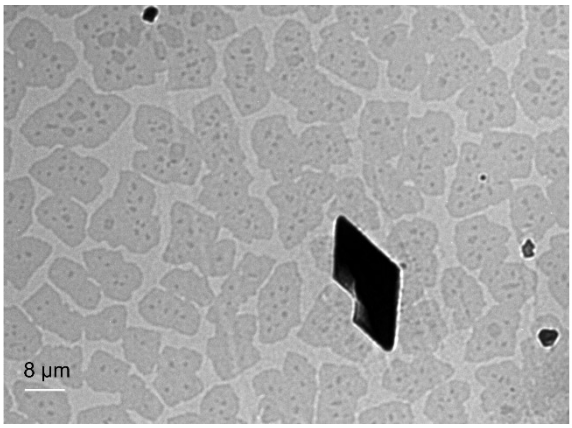

Figure S18. TEM images of Na-Ti_2Nb_8.

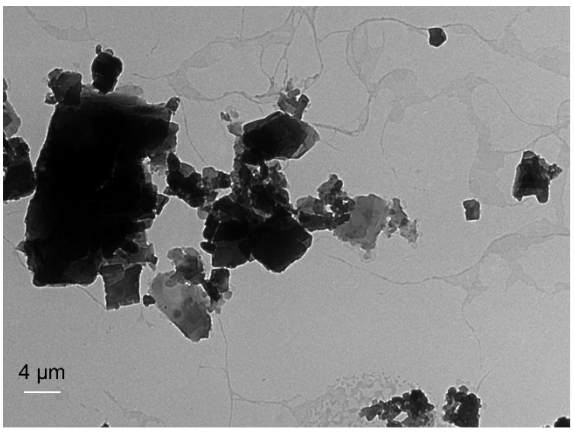

Figure S19. TEM images of Co-Nb_6.

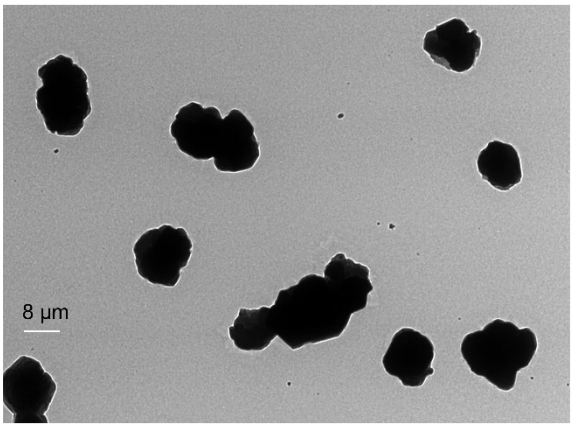

Figure S20. TEM images of $Co(en)_3ClSO_4$.

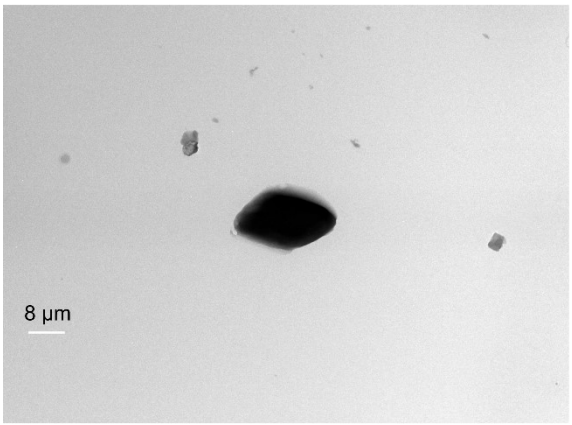

Figure S21. TEM images of $Co(OAc)_2$.

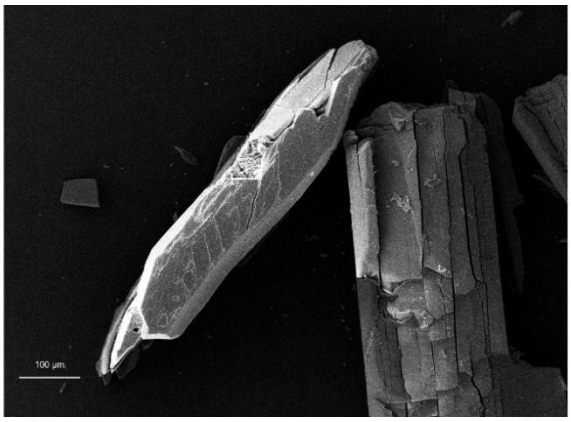

Figure S22. SEM images of Co-Ti_2Nb_8.

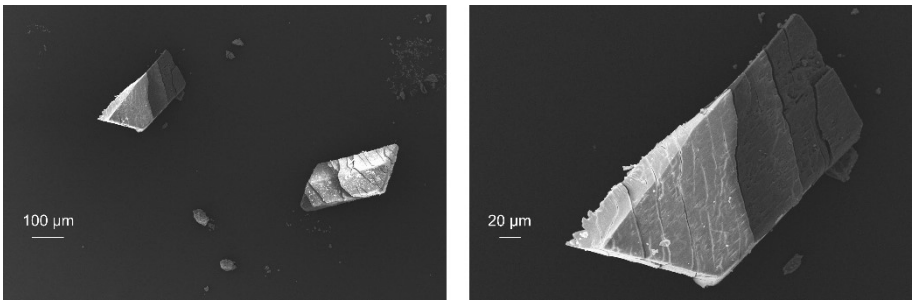

Figure S23. SEM images of Cu-Ti_2Nb_8.

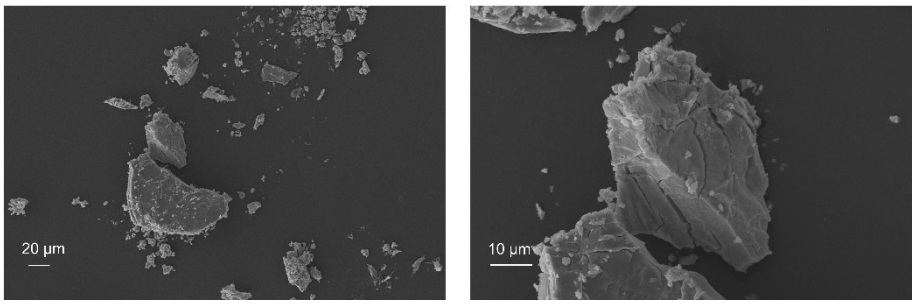

Figure S24. SEM images of Na-Ti_2Nb_8.

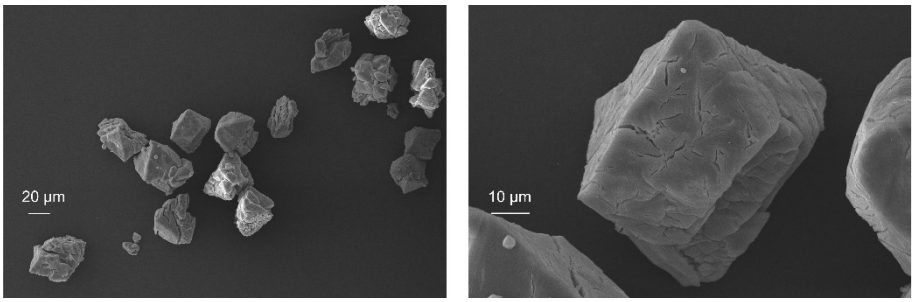

Figure S25. SEM images of Co-Nb_6.

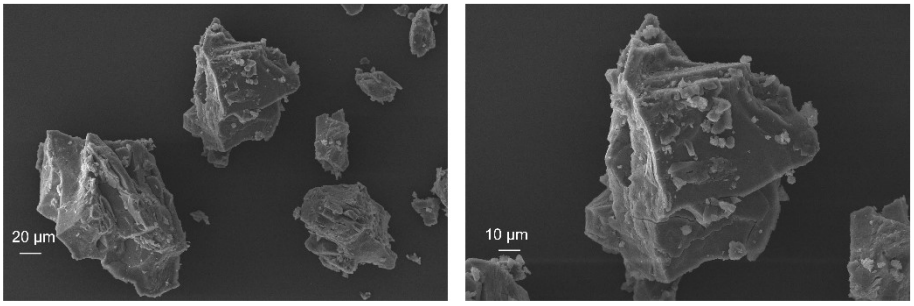

Figure S26. SEM images of $Co(en)_3ClSO_4$.

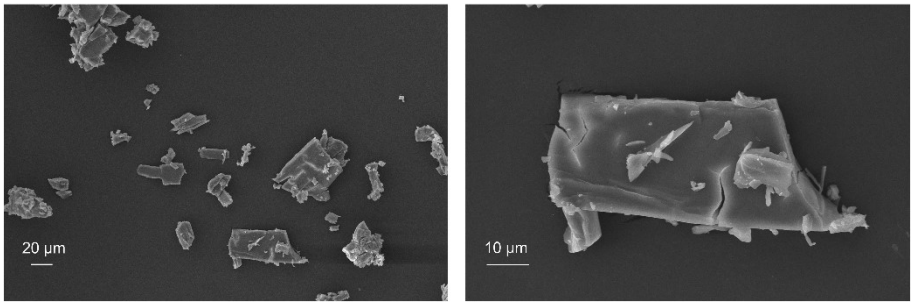

Figure S27. SEM images of $Co(OAc)_2$.

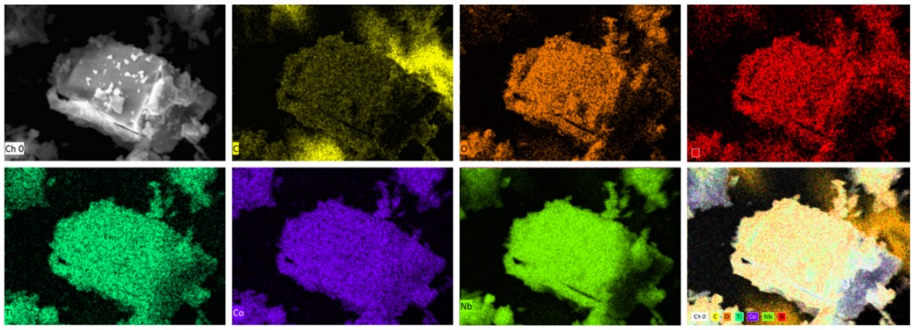

Figure S28. EDS elemental mapping images of C, O, N, Ti, Co and Nb of Co-Ti_2Nb_8.

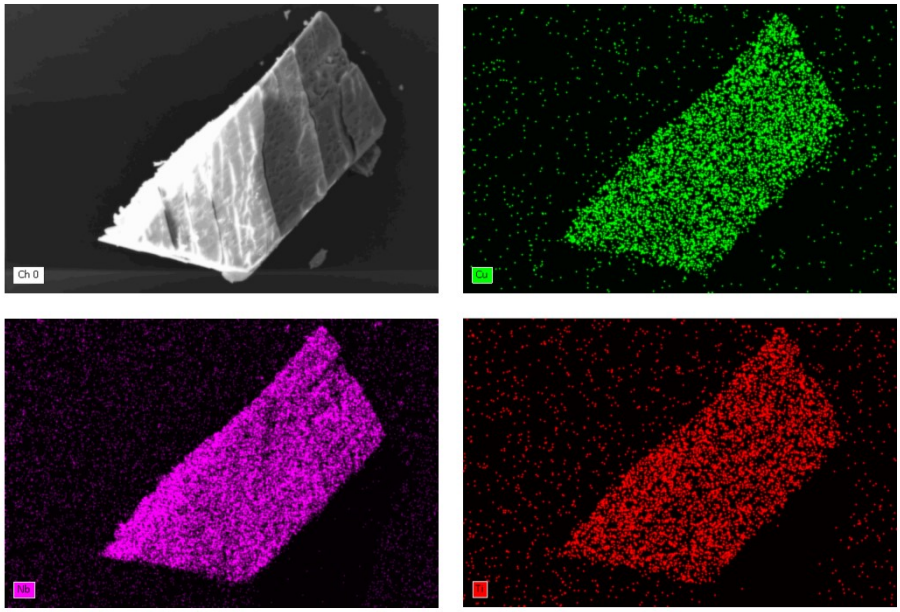

Figure S29. EDS elemental mapping images of Cu, Nb and Ti of Cu-Ti_2Nb_8.

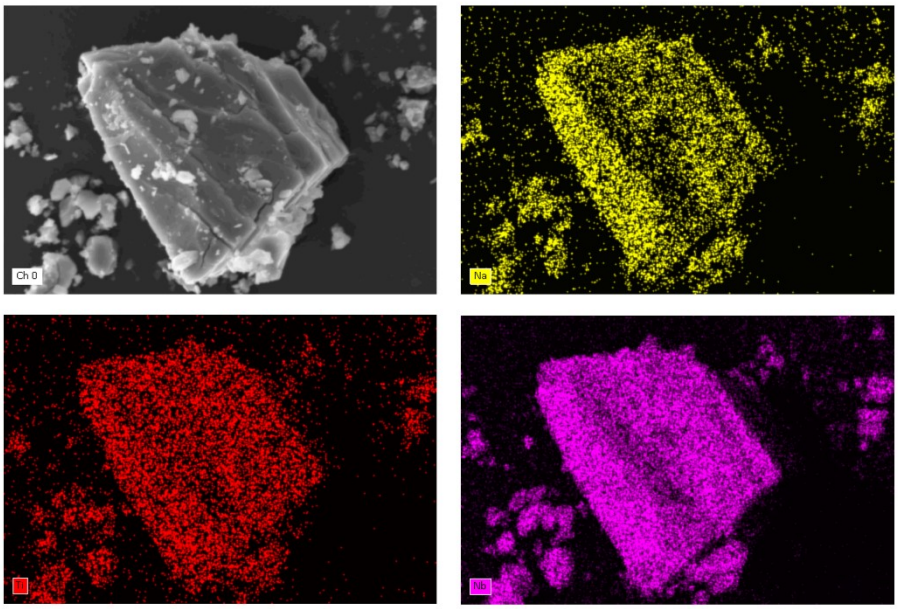

Figure S30. EDS elemental mapping images of Na, Nb and Ti of Na-Ti_2Nb_8.

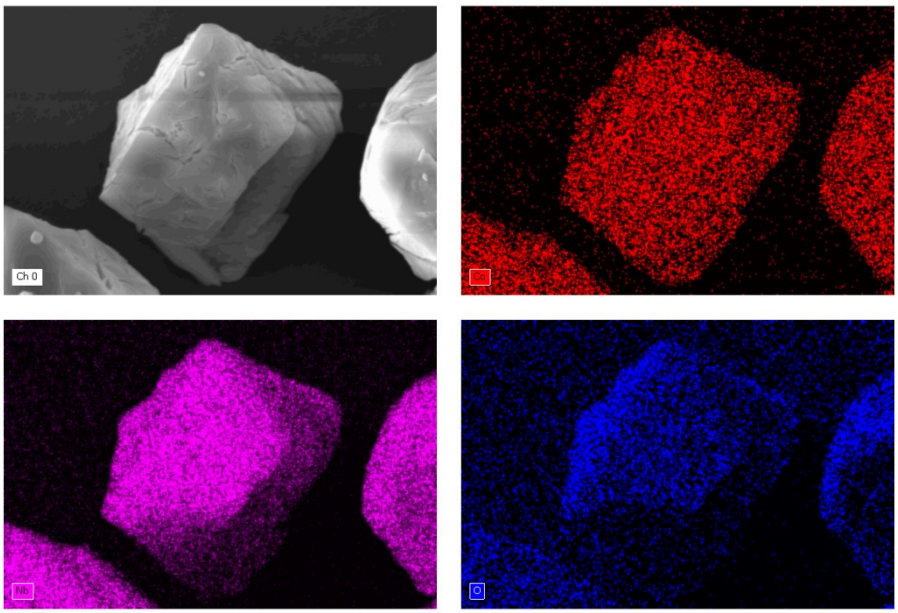

Figure S31. EDS elemental mapping images of Co, Nb and O of Co-Nb_6.

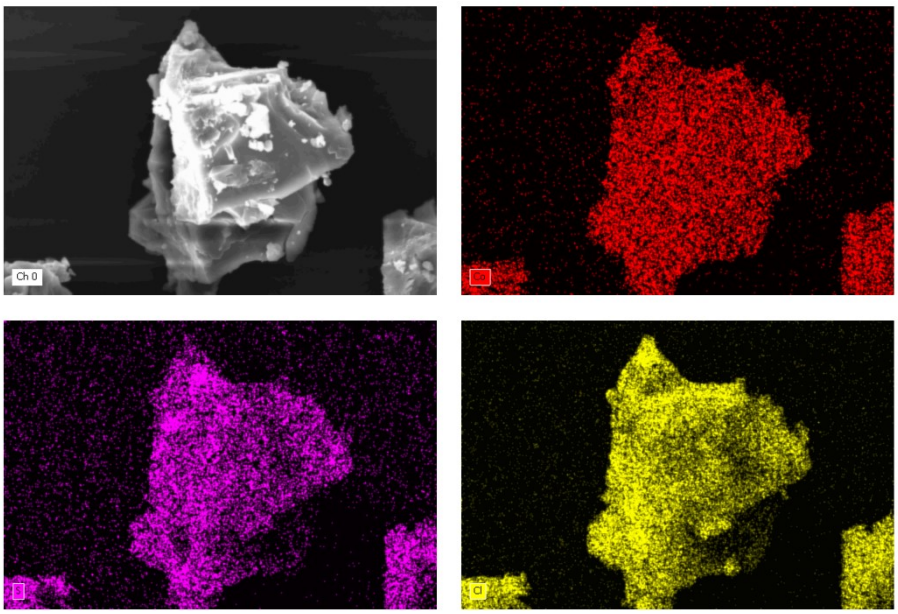

Figure S32. EDS elemental mapping images of Co, S and Cl of $Co(en)_3ClSO_4$.

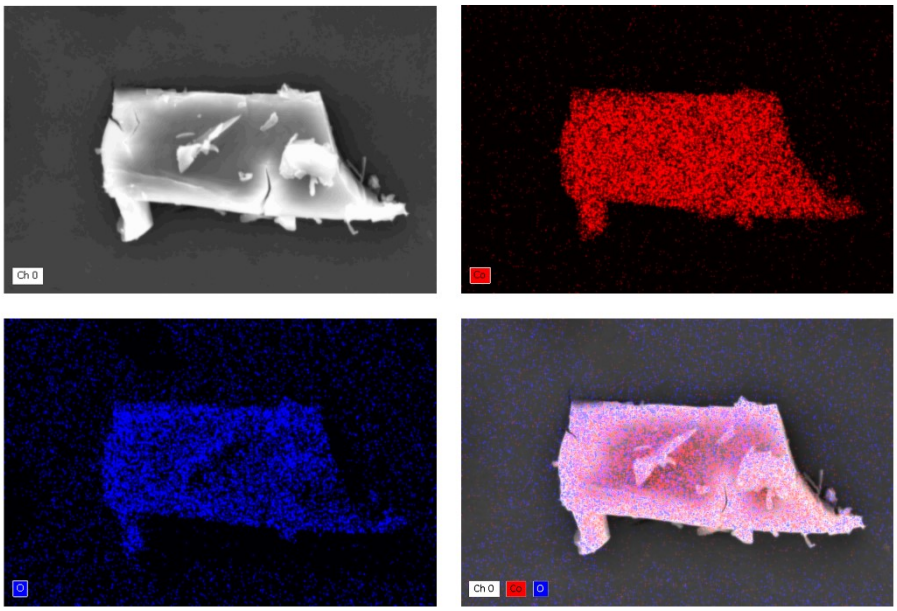

Figure S33. EDS elemental mapping images of Co and O of $Co(OAc)_2$.

Table S8. BET surface area of catalysts

Catalysts	BET surface area (m^2/g)
Co-Ti_2Nb_8	2.96
Cu-Ti_2Nb_8	5.22
Na-Ti_2Nb_8	2.72
Co-Nb_6	5.07
$Co(en)_3ClSO_4$	2.41
$Co(OAc)_2$	5.25

Note: measured at 77K.

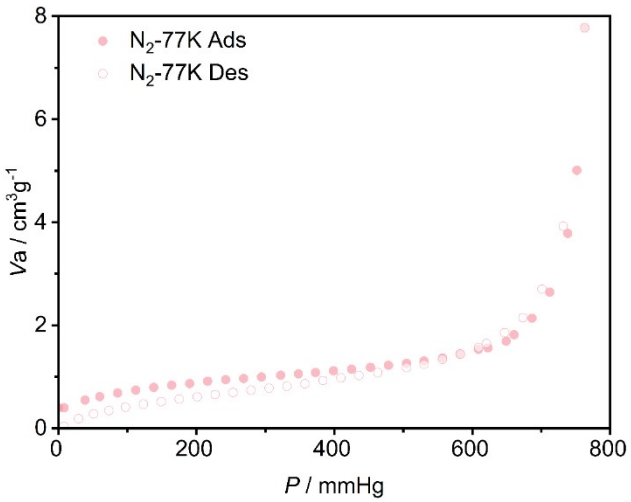

Figure S34. The nitrogen adsorption curve of Co-Ti_2Nb_8 was measured at 77K.

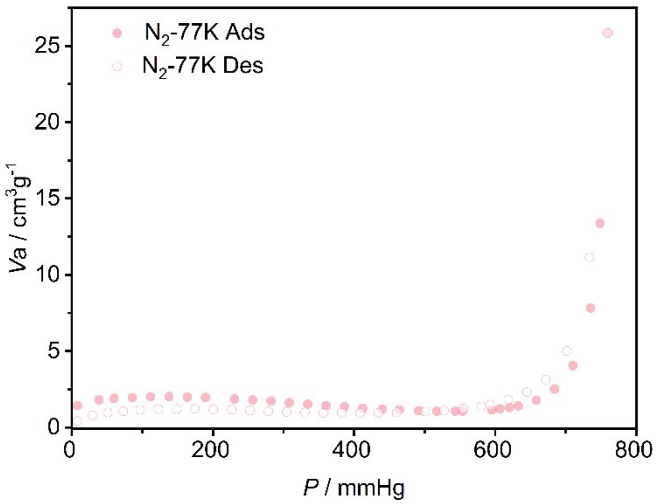

Figure S35. The nitrogen adsorption curve of Cu-Ti_2Nb_8 was measured at 77K.

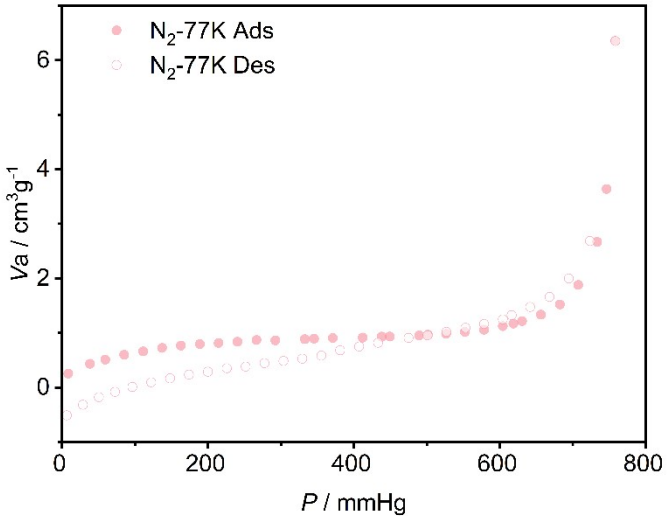

Figure S36. The nitrogen adsorption curve of Na-Ti_2Nb_8 was measured at 77K.

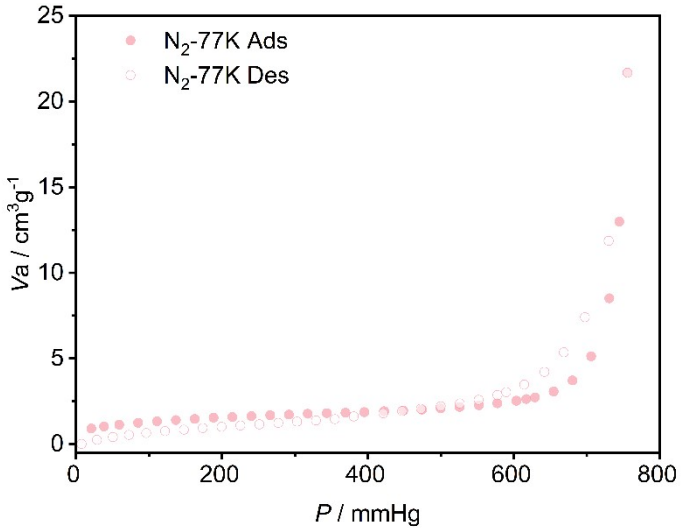

Figure S37. The nitrogen adsorption curve of Co-Nb_6 was measured at 77K.

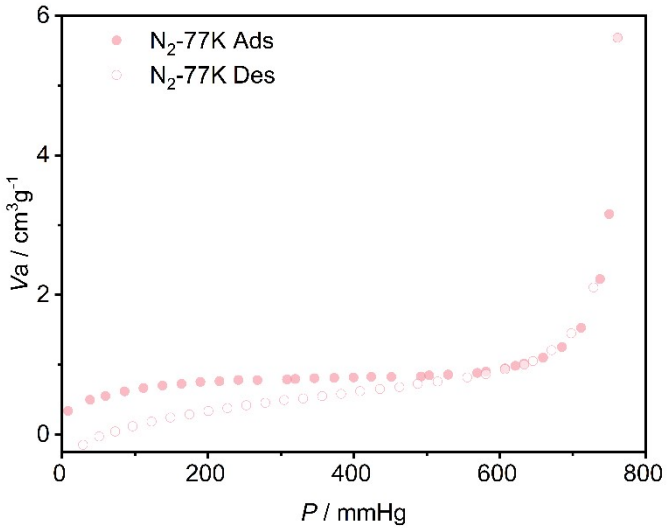

Figure S38. The nitrogen adsorption curve of $Co(en)_3ClSO_4$ was measured at 77K.

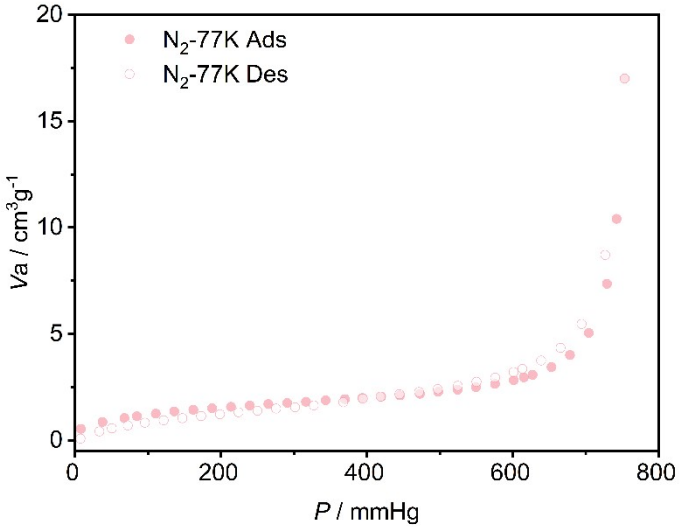

Figure S39. The nitrogen adsorption curve of $Co(OAc)_2$ was measured at 77K.

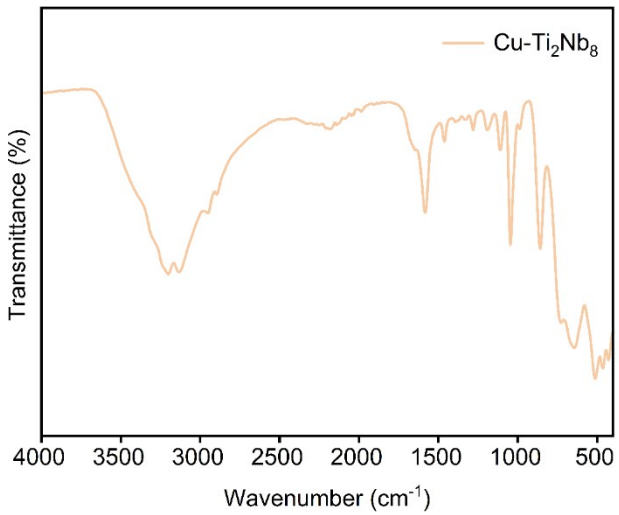

Figure S40. IR spectrum of Cu-Ti_2Nb_8.

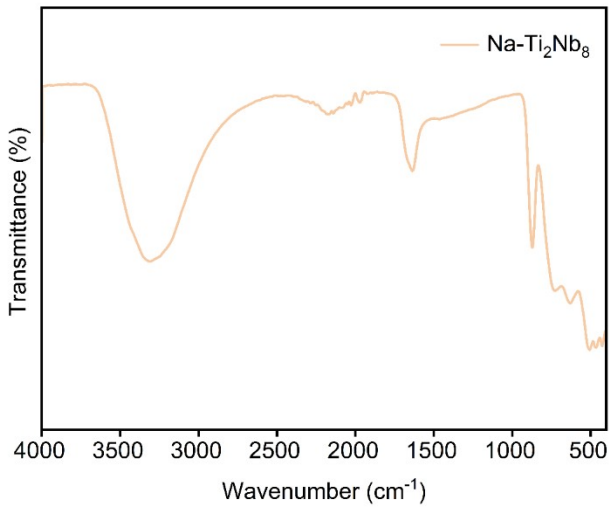

Figure S41. IR spectrum of Na-Ti_2Nb_8.

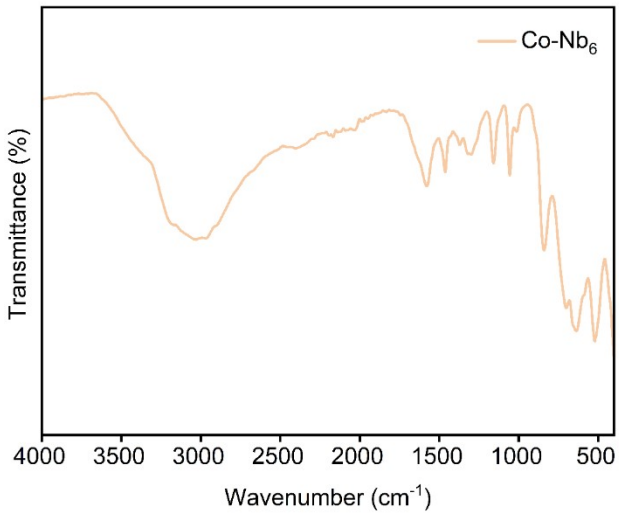

Figure S42. IR spectrum of Co-Nb_6.

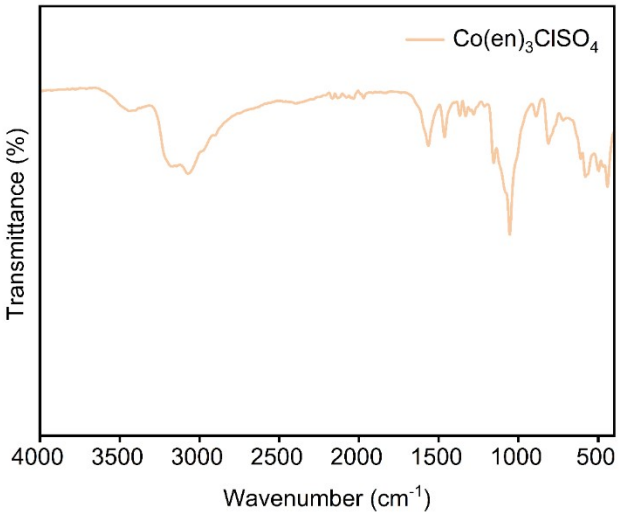

Figure S43. IR spectrum of $Co(en)_3ClSO_4$.

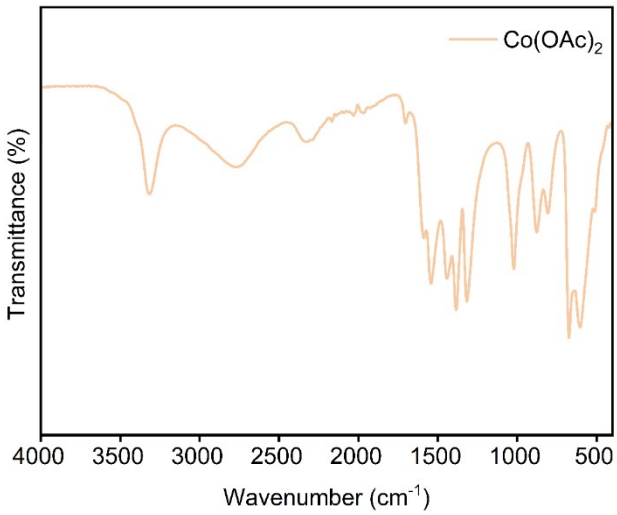

Figure S44. IR spectrum of $Co(OAc)_2$.

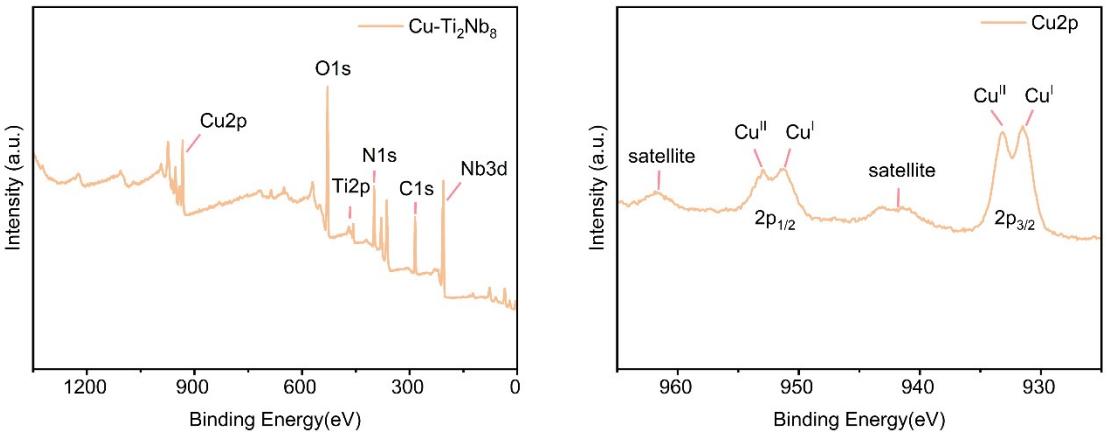

Figure S45. The XPS spectra of Cu-Ti_2Nb_8.

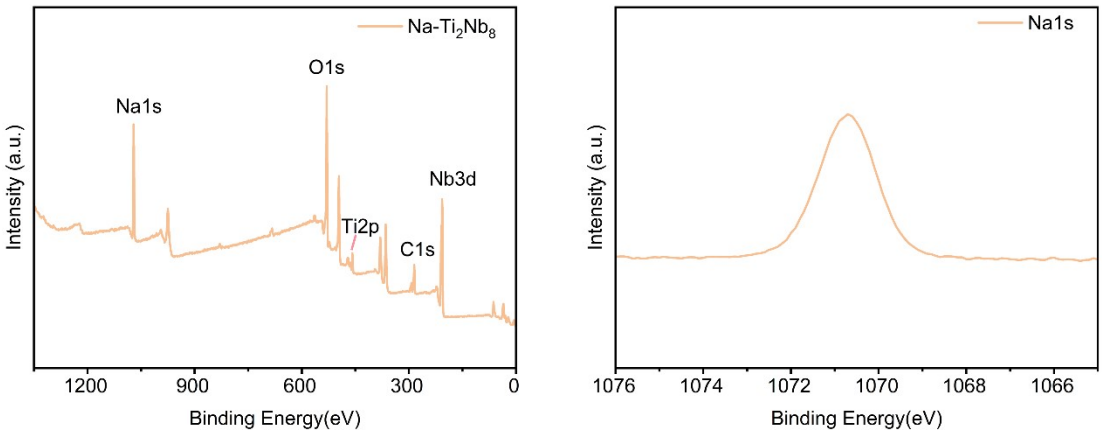

Figure S46. The XPS spectra of Na-Ti_2Nb_8.

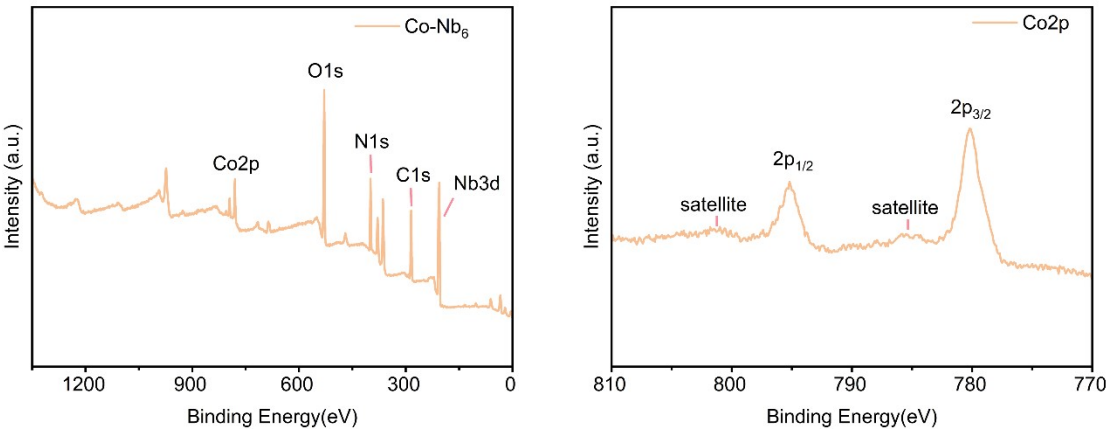

Figure S47. The XPS spectra of Co-Nb_6.

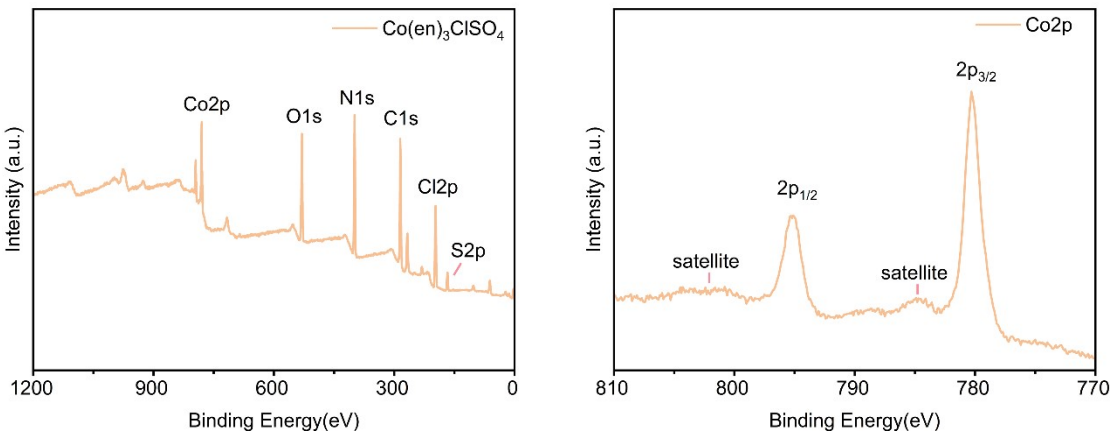

Figure S48. The XPS spectra of $Co(en)_3ClSO_4$.

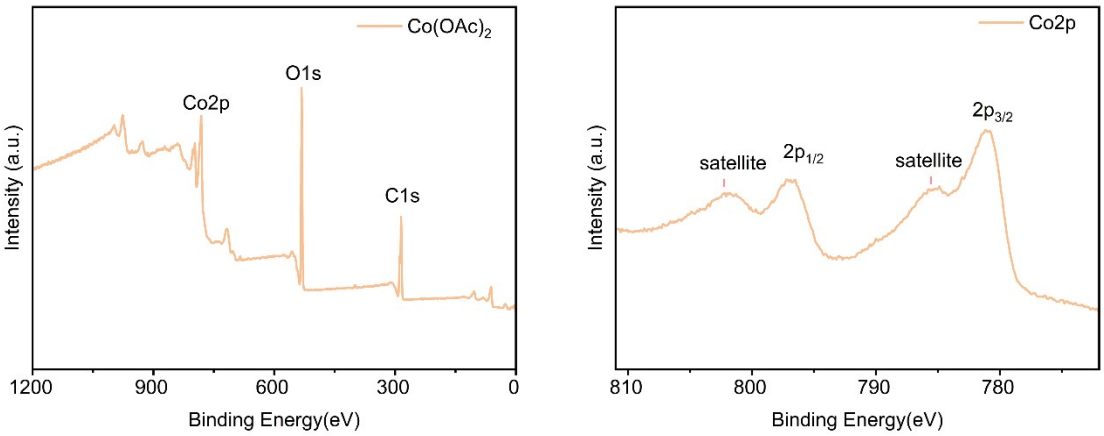

Figure S49. The XPS spectra of $Co(OAc)_2$.

8. Calculation Section

First-principles DFT simulations were performed using the VASP package. The electron exchange-correlation (XC) energies were treated by the generalized gradient approximation (GGA) in the Perdew Burke Ernzerhof (PBE) scheme.[5] In addition, the projection enhanced wave (PAW) pseudopotential was used to describe the ion nucleus and valence electron interactions.[6] A kinetic energy cutoff of 400 eV was chosen as the plane wave basis set. To focus solely on the interactions between the oxygen molecules and the active sites, we simplified the calculations and reduced the computational load by extracting the Co-Ti_2Nb_8 dimer as the computational model. Under the premise of immobilizing the niobium-oxo cluster components, the adsorption of oxygen and its interaction with the cobalt complex active center were optimized, with the forces fell below 0.01 eV $Å^{-1}$. The integration over the reciprocal space was performed using a Monkhorst model with a Γ-point. The atomistic structures and the difference charge densities are illustrated using VESTA.[7] The version of the Bader program used for Bader charge analysis is v1.05.[8]

9. References

1. C. X. Chen, S. L. Duan, X. Y. Zhang, R. Z. Sun, P. W. Cai, C. Sun and S. T. Zheng, *Dalton Trans*. **2025**, DOI: 10.1039/D4DT03071K.

2. Y. T. Zhang, P. Huang, C. Qin, L. K. Yan, B. Q. Song, Z. X. Yang, K. Z. Shao and Z. M. Su, *Dalton Trans.* **2014**, *43*, 9847–9850.

3. M. Nyman, L. J. Criscenti, F. Bonhomme, M. A. Rodriguez, R. T. Cygan, *J. Solid State Chem.* **2003**, *176*, 111–119.

4. D. Jacewicz, J. Pranczk, D. Wyrzykowski, K. Żamojć, L. Chmurzyński, *React. Kinet. Mech. Catal.* **2014**, *113*, 321–331.

5. J. P. Perdew, K. Burke, M. Ernzerhof, *Phys. Rev. Lett.* ***1996,*** 77, 3865–3868.

6. a) P. E. Blochl. *Phys. Rev. B* ***1994****, 50, 17953*–17979; b) G. Kresse, D. Joubert, *Phys. Rev. B* ***1999****, 59,* 1758–1775.

7. K. Momma, F. Izumi, *J. Appl. Crystallogr*. **2011**, *44*, 1272–1276.

8. W. Tang, E. Sanville, G. Henkelman, *J. Phys.: Condens. Matter* **2009**, *21*, 084204.

10. ^{1}H and ^{13}C NMR Spectra

2a–^{1}H NMR–DMSO-d6

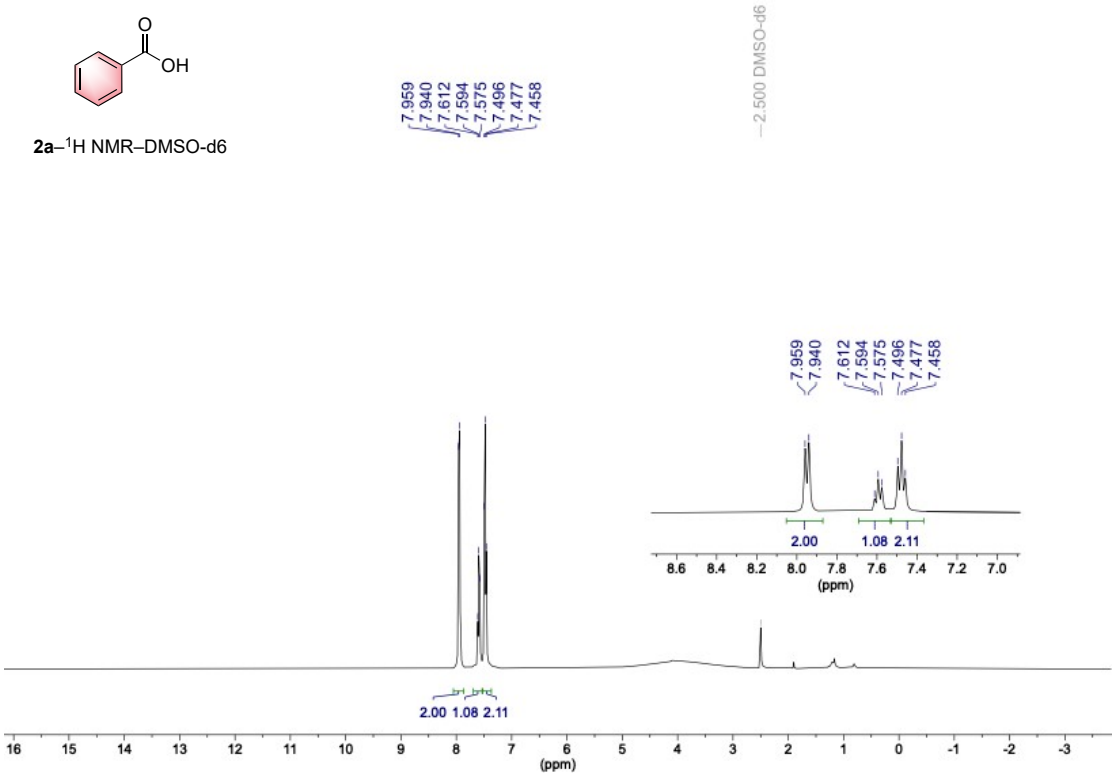

2a–^{13}C NMR–DMSO-d6

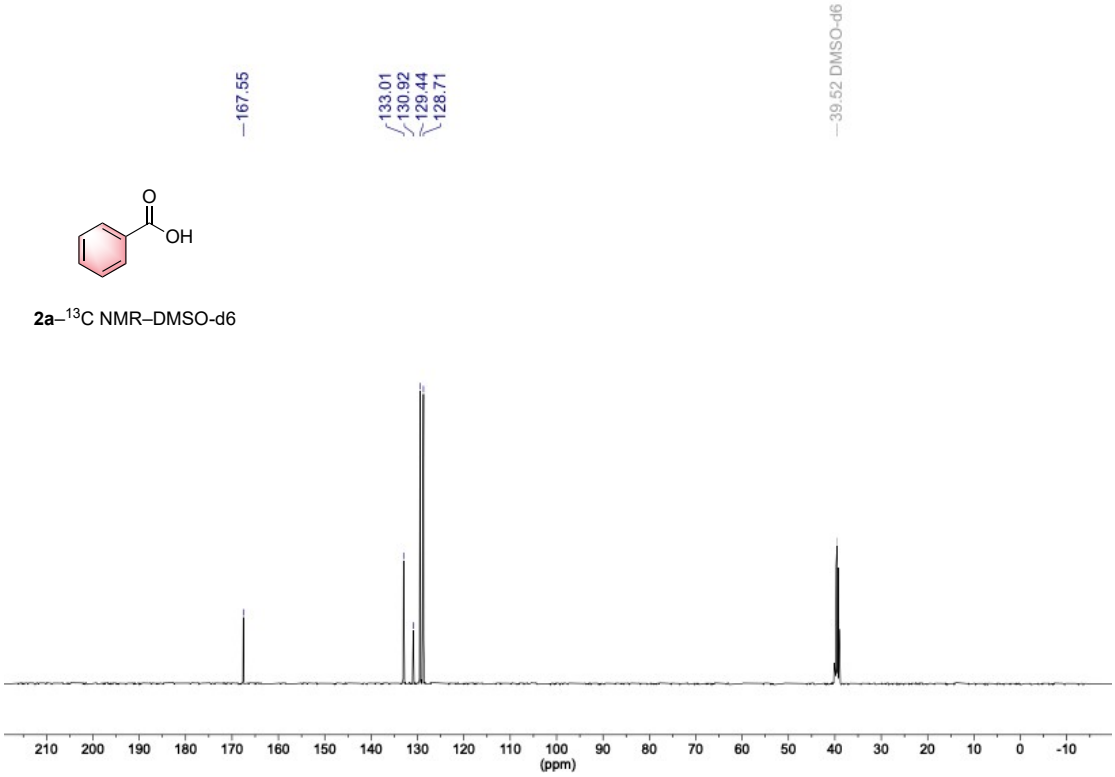

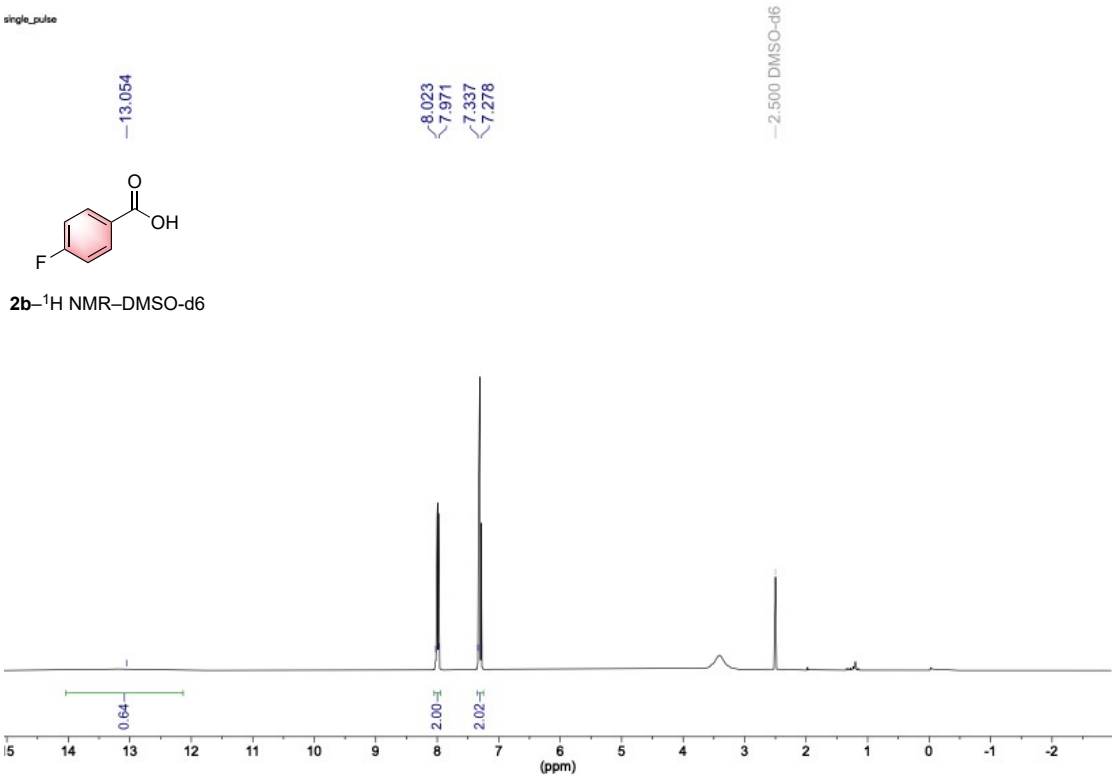

2b–^{1}H NMR–DMSO-d6

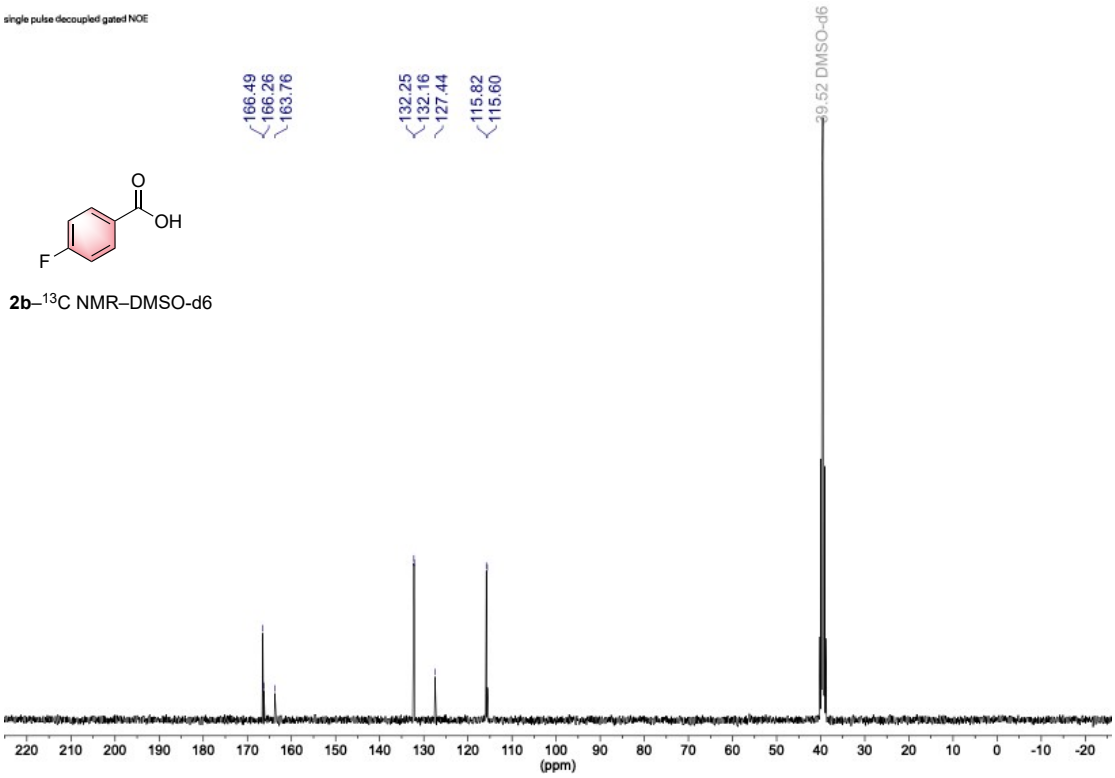

2b–^{13}C NMR–DMSO-d6

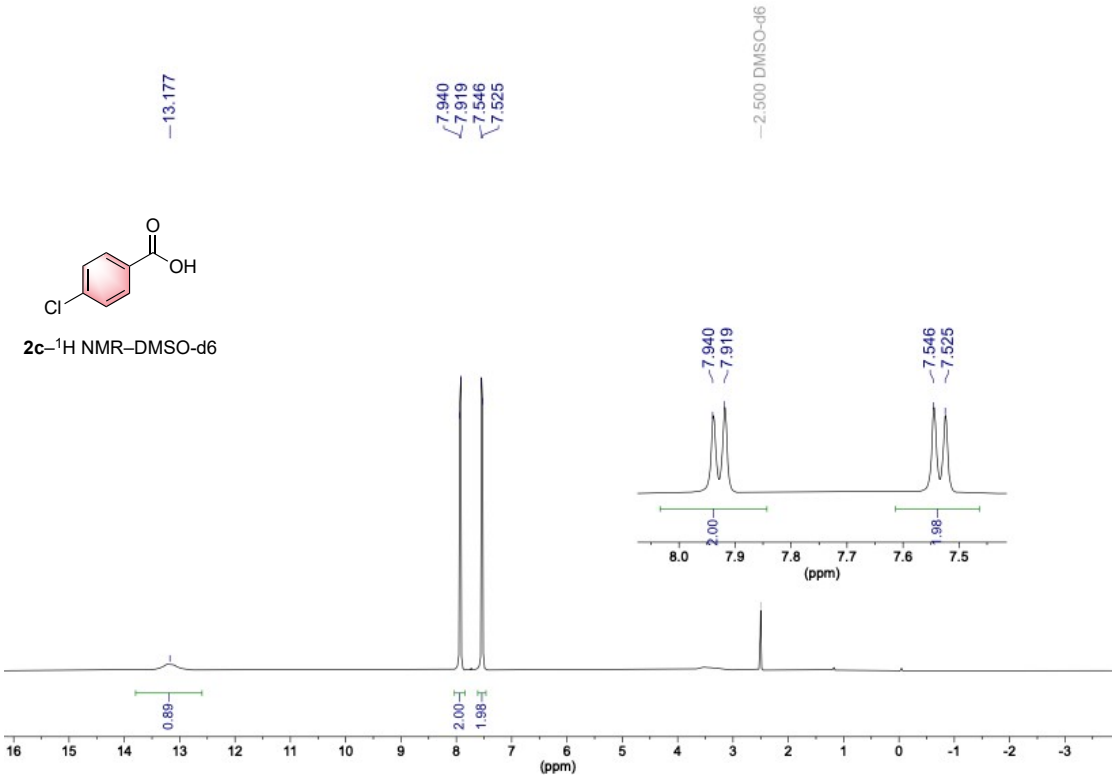

2c–^{1}H NMR–DMSO-d6

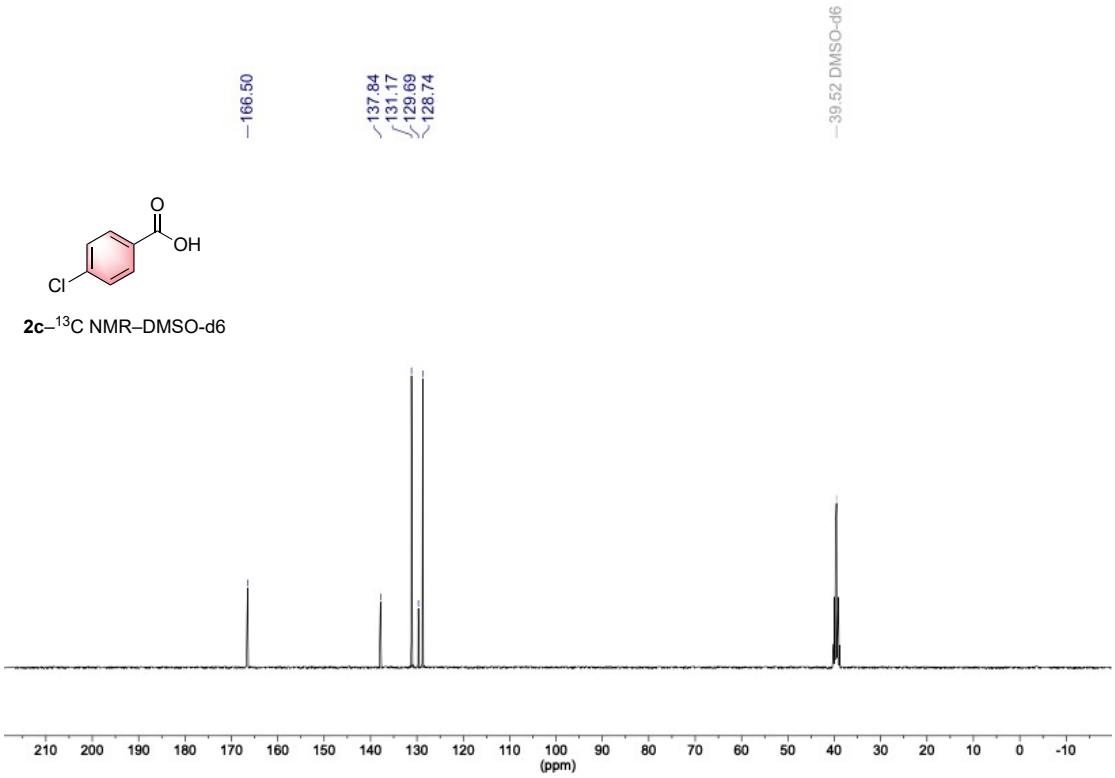

2c–^{13}C NMR–DMSO-d6

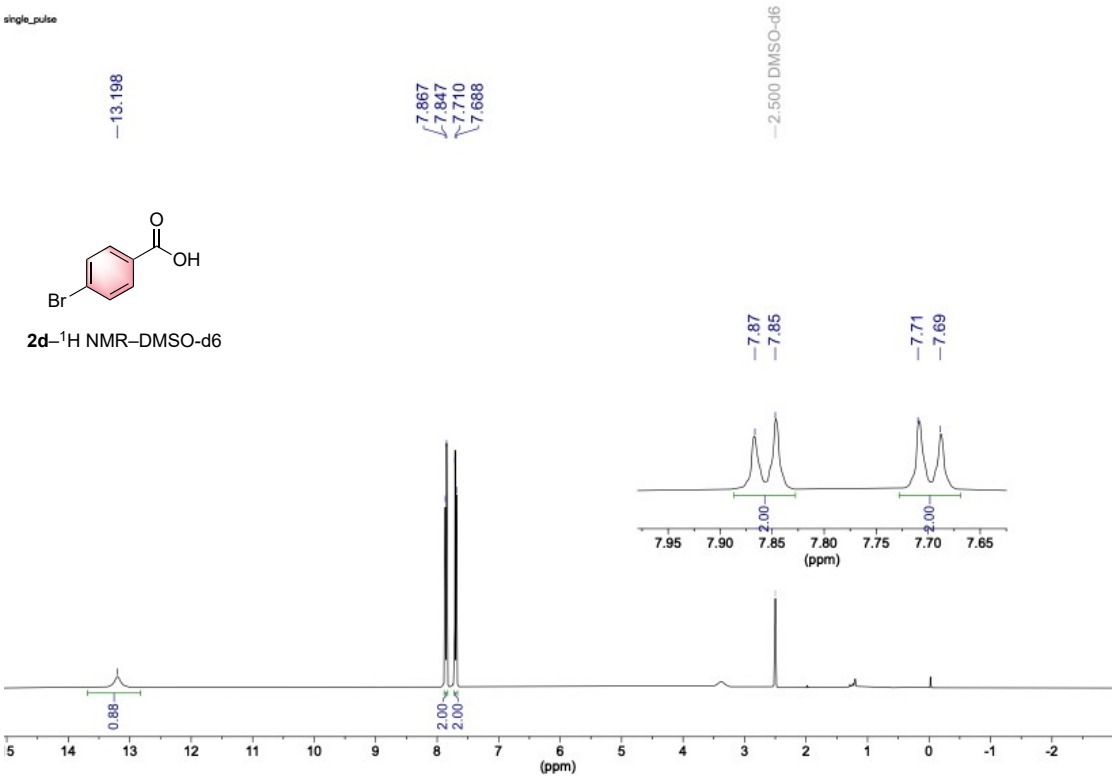

2d–^{1}H NMR–DMSO-d6

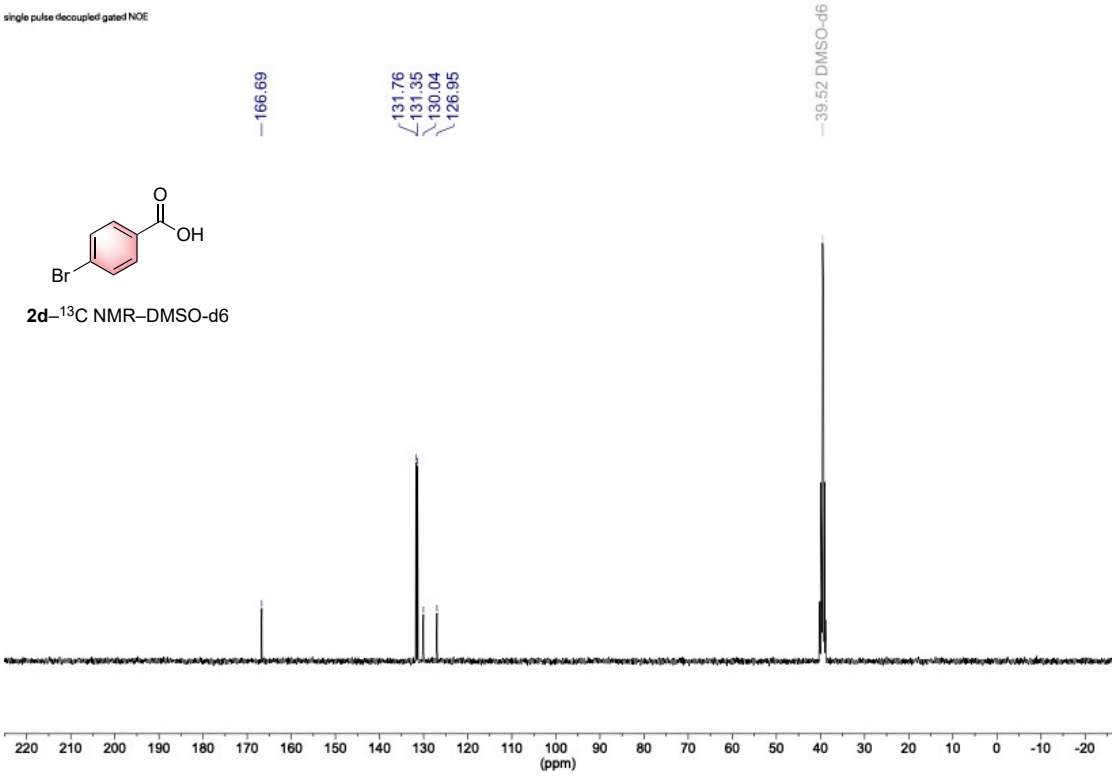

2d–^{13}C NMR–DMSO-d6

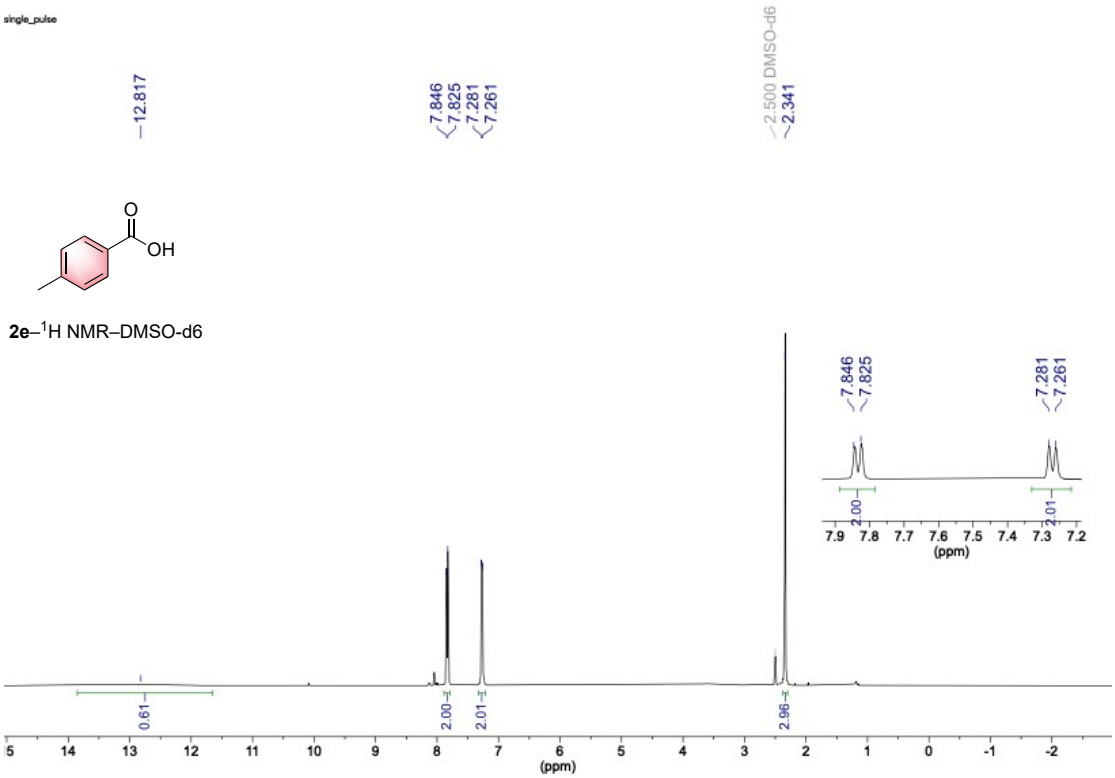

2e–^{1}H NMR–DMSO-d6

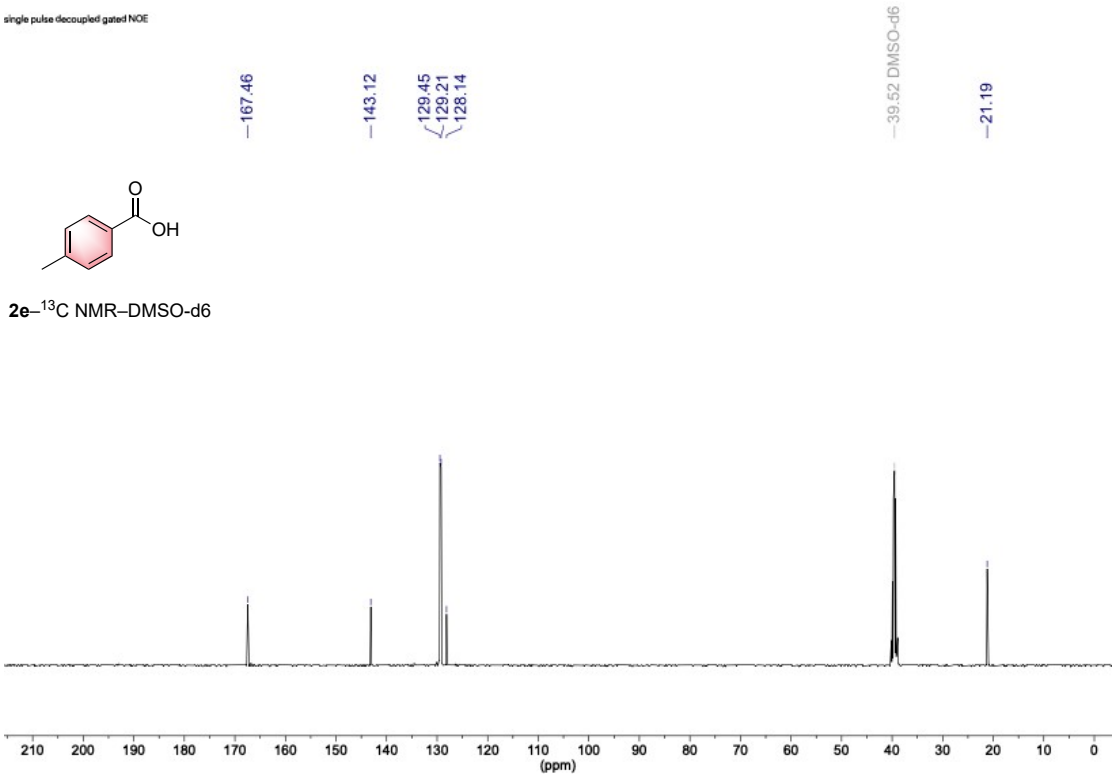

2e–^{13}C NMR–DMSO-d6

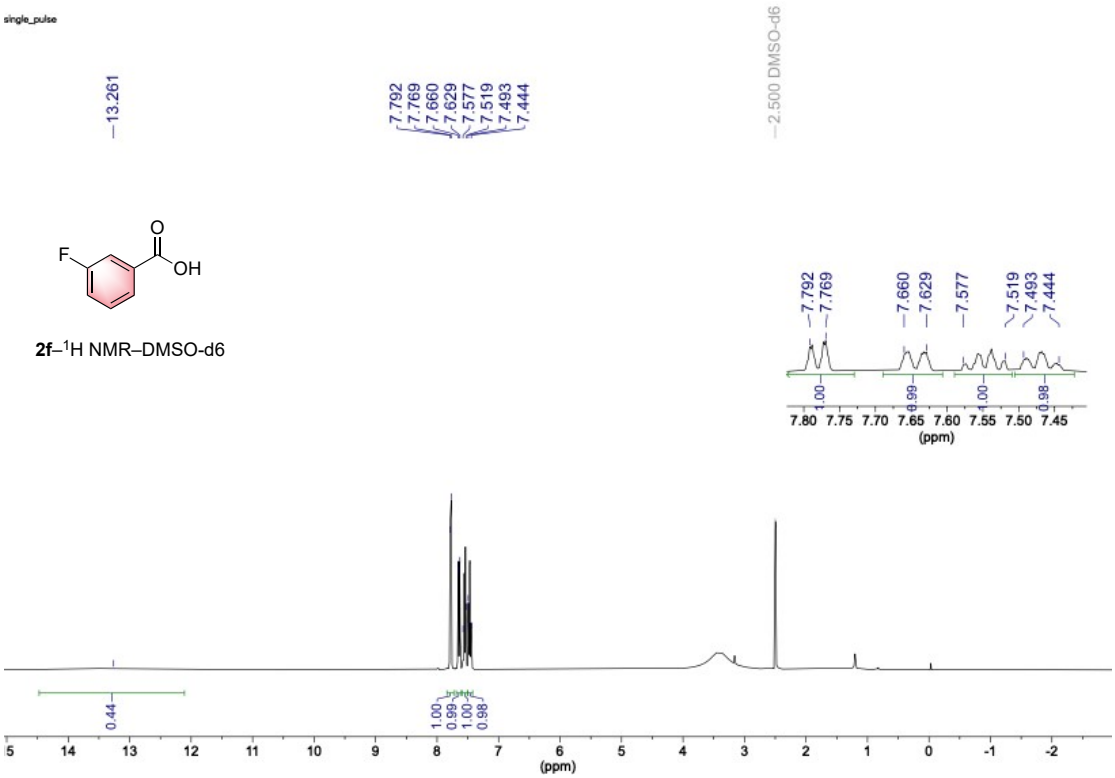

2f–^{1}H NMR–DMSO-d6

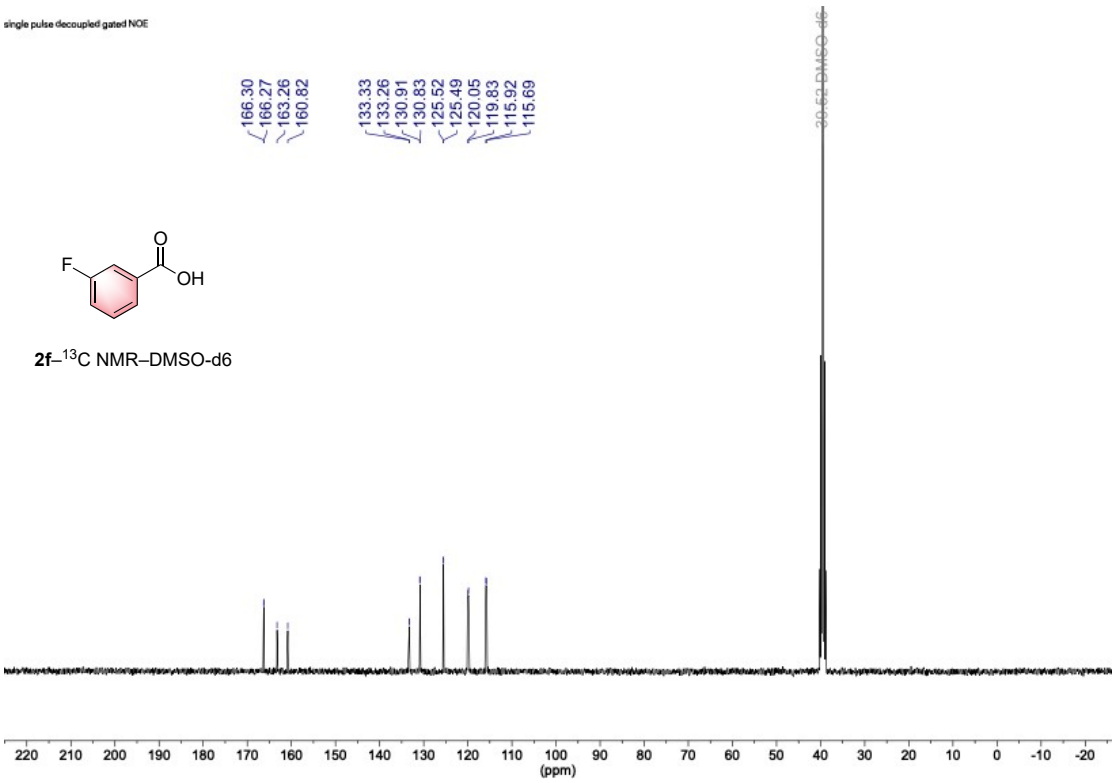

2f–^{13}C NMR–DMSO-d6

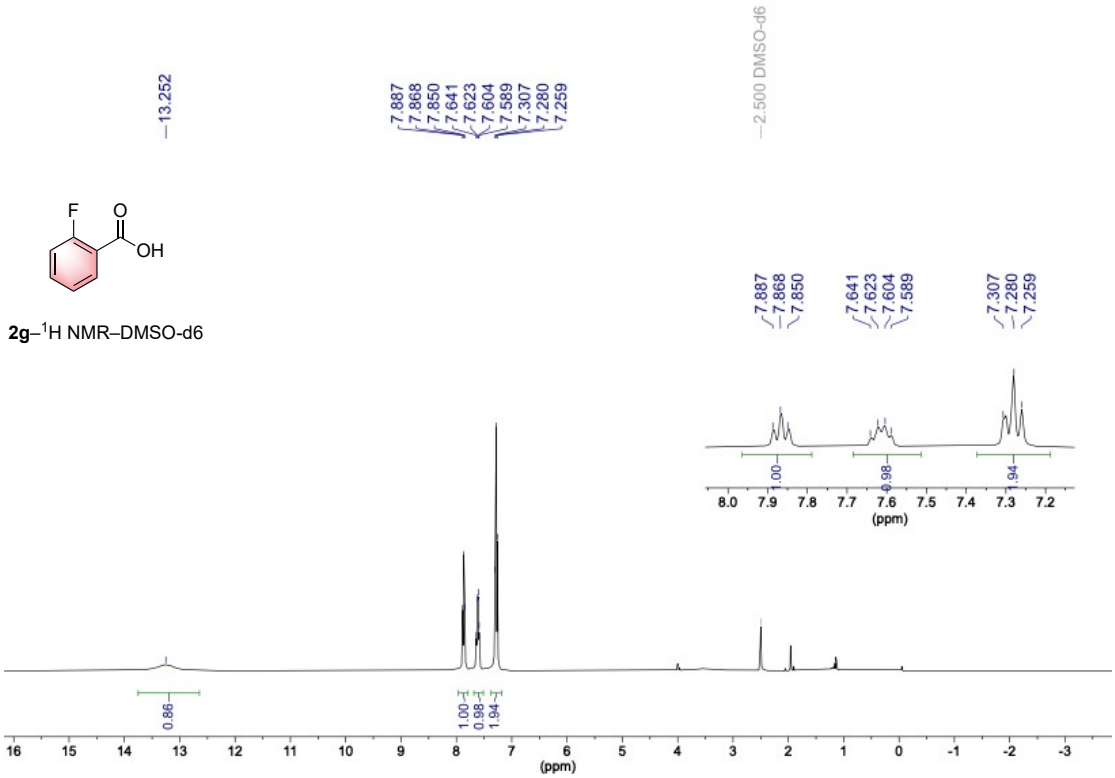

2g–^{1}H NMR–DMSO-d6

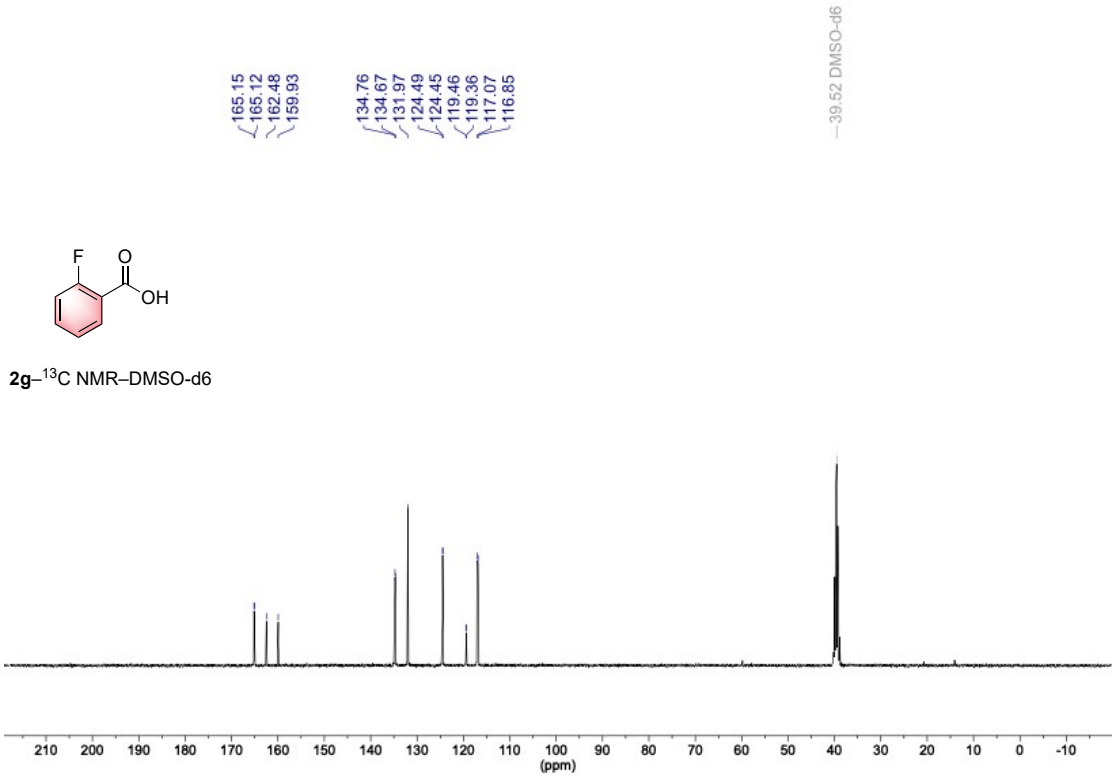

2g–^{13}C NMR–DMSO-d6

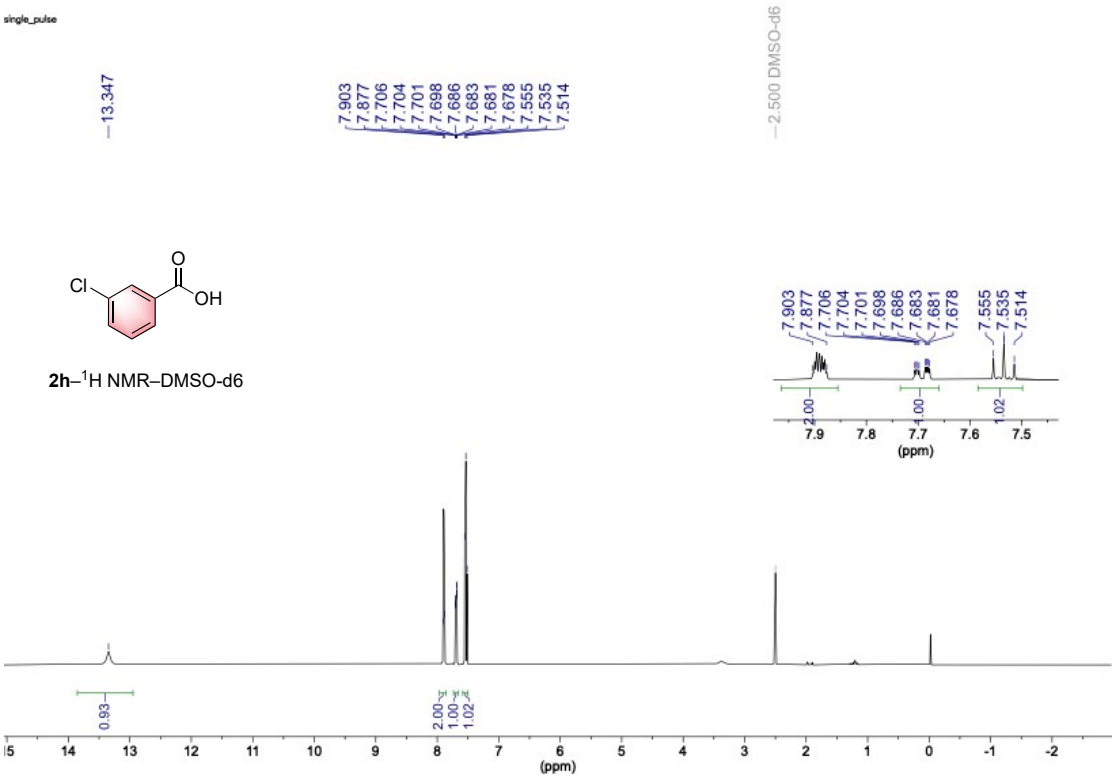
single_pulse
13.347
7.903
7.877
7.706
7.704
7.701
7.698
7.686
7.683
7.681
7.678
7.555
7.535
7.514
2.500 DMSO-d6
Cl
O
OH
2h–1H NMR–DMSO-d6
0.93
2.00
1.00
1.02
(ppm)

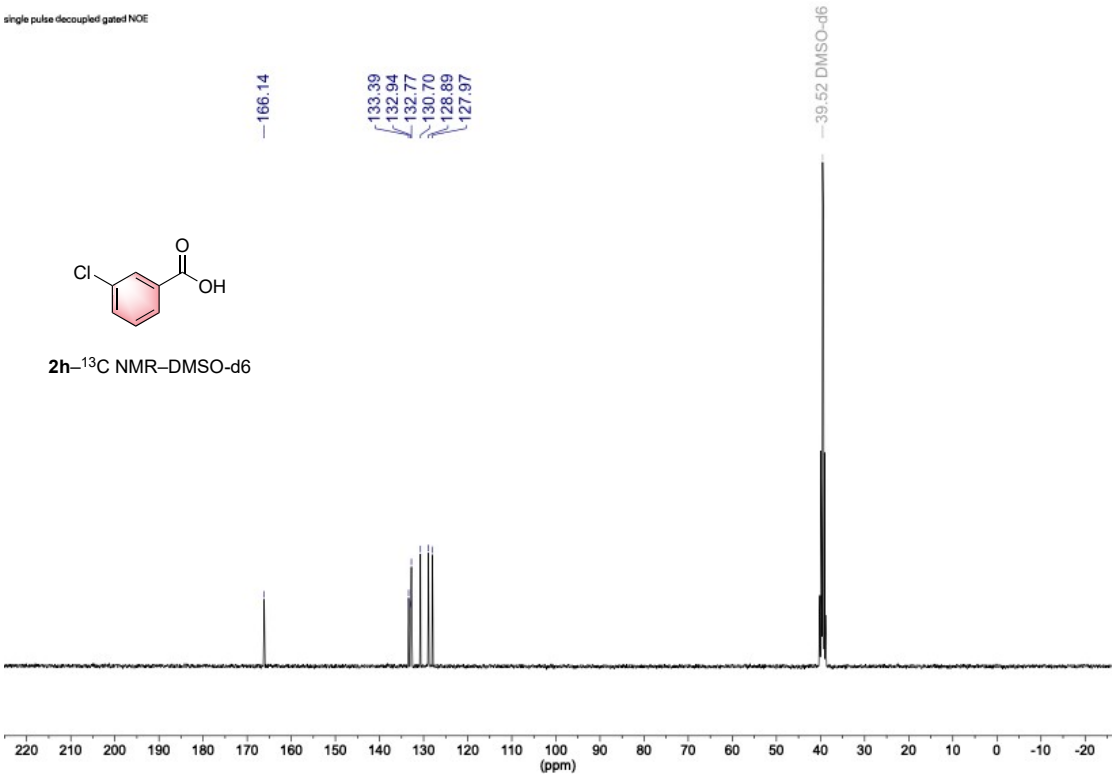
single pulse decoupled gated NOE
166.14
133.39
132.94
132.77
130.70
128.89
127.97
39.52 DMSO-d6
Cl
O
OH
2h–13C NMR–DMSO-d6
(ppm)

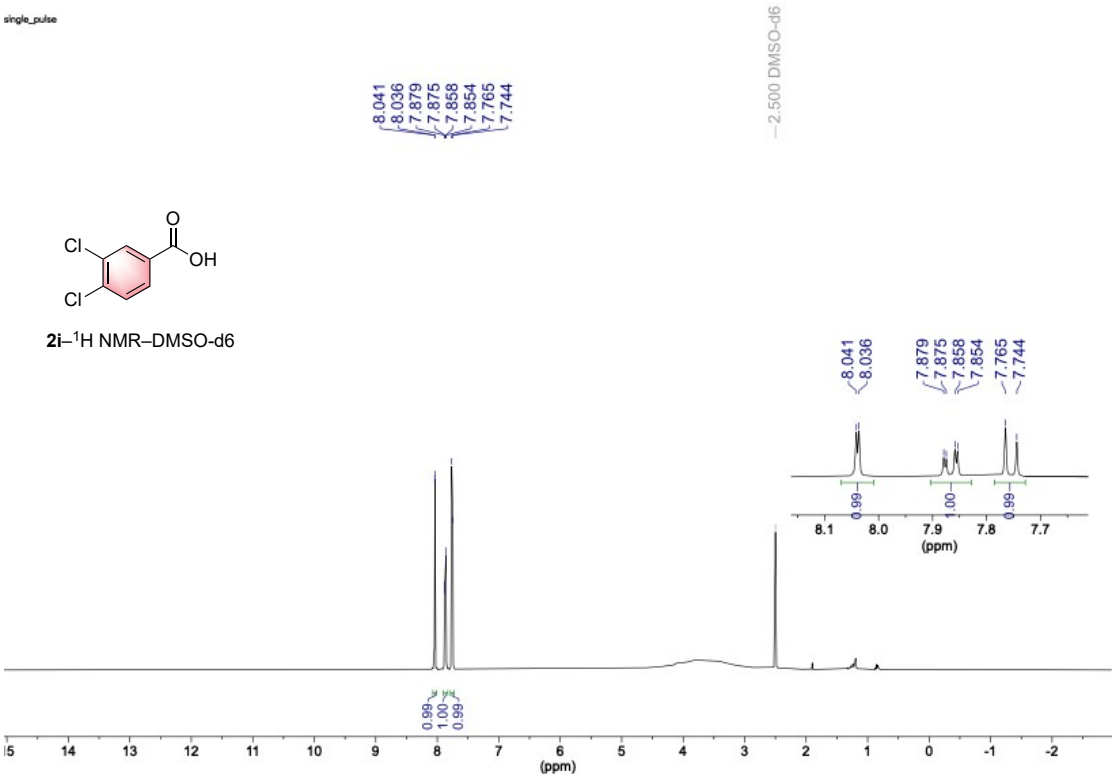

2i–^{1}H NMR–DMSO-d6

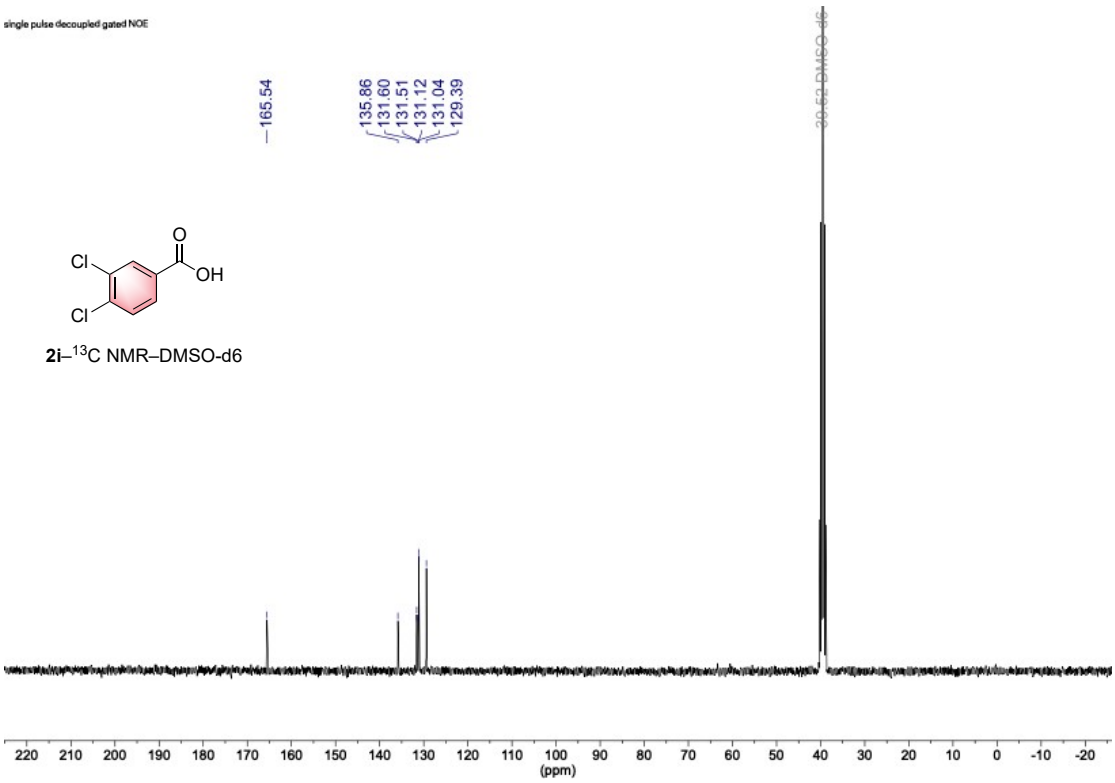

2i–^{13}C NMR–DMSO-d6

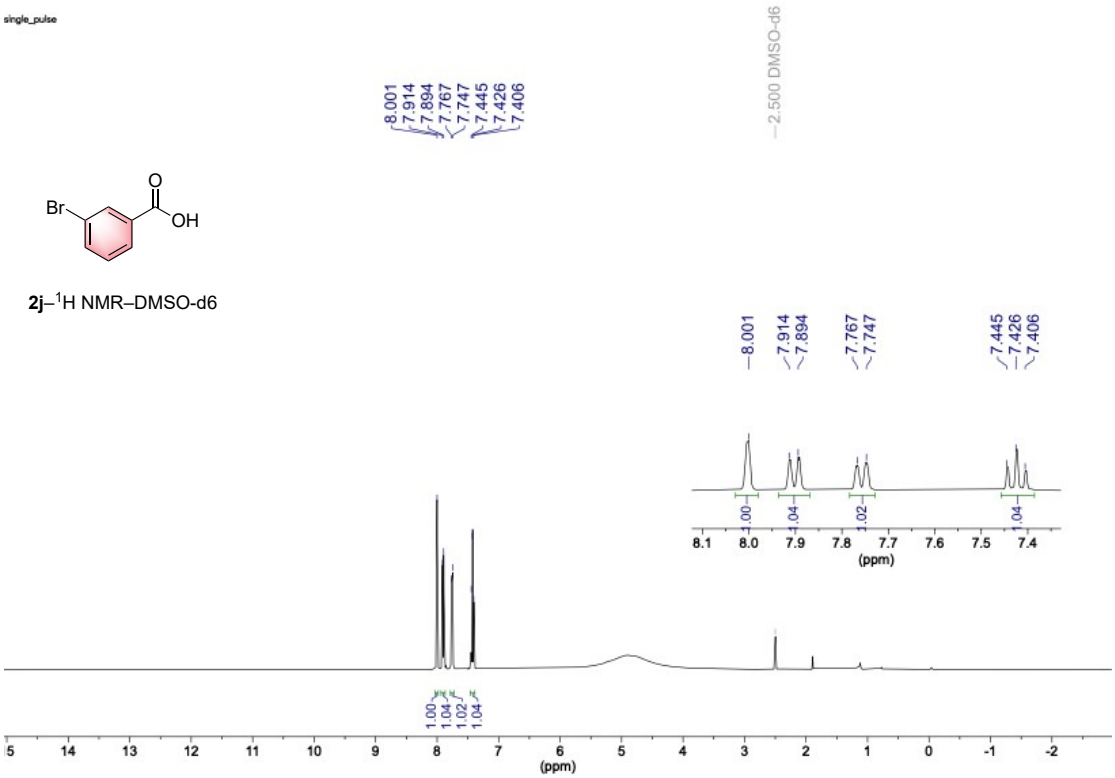

2j–^{1}H NMR–DMSO-d6

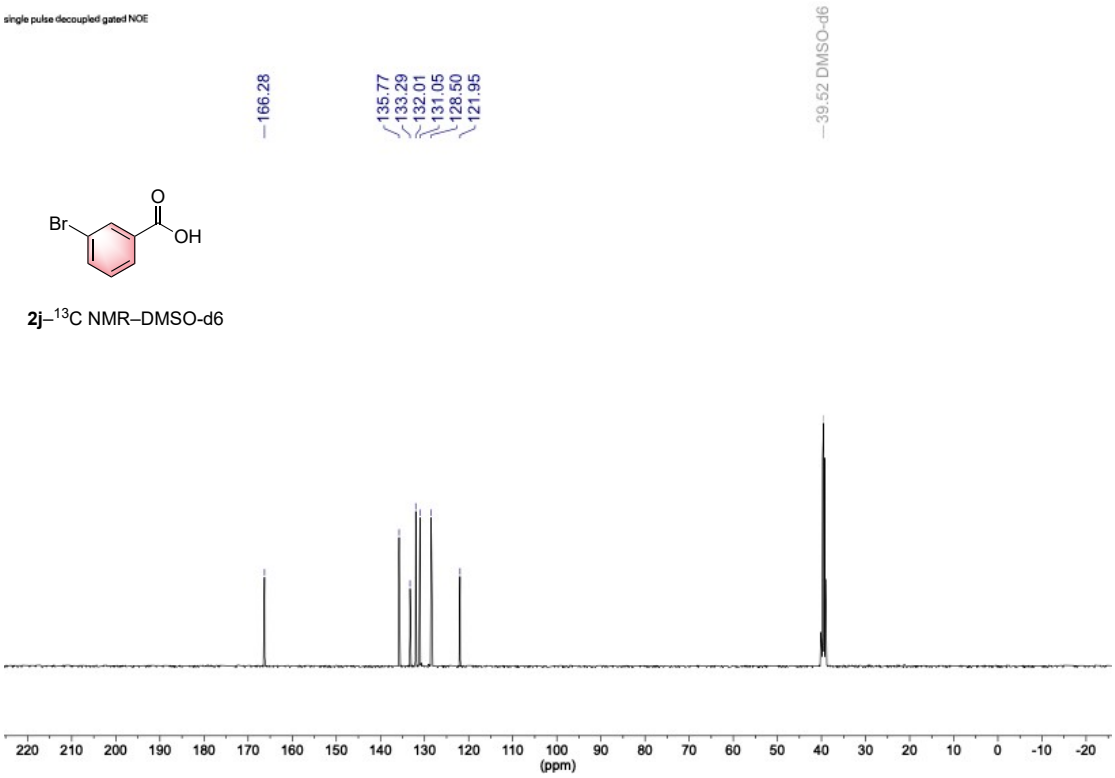

2j–^{13}C NMR–DMSO-d6

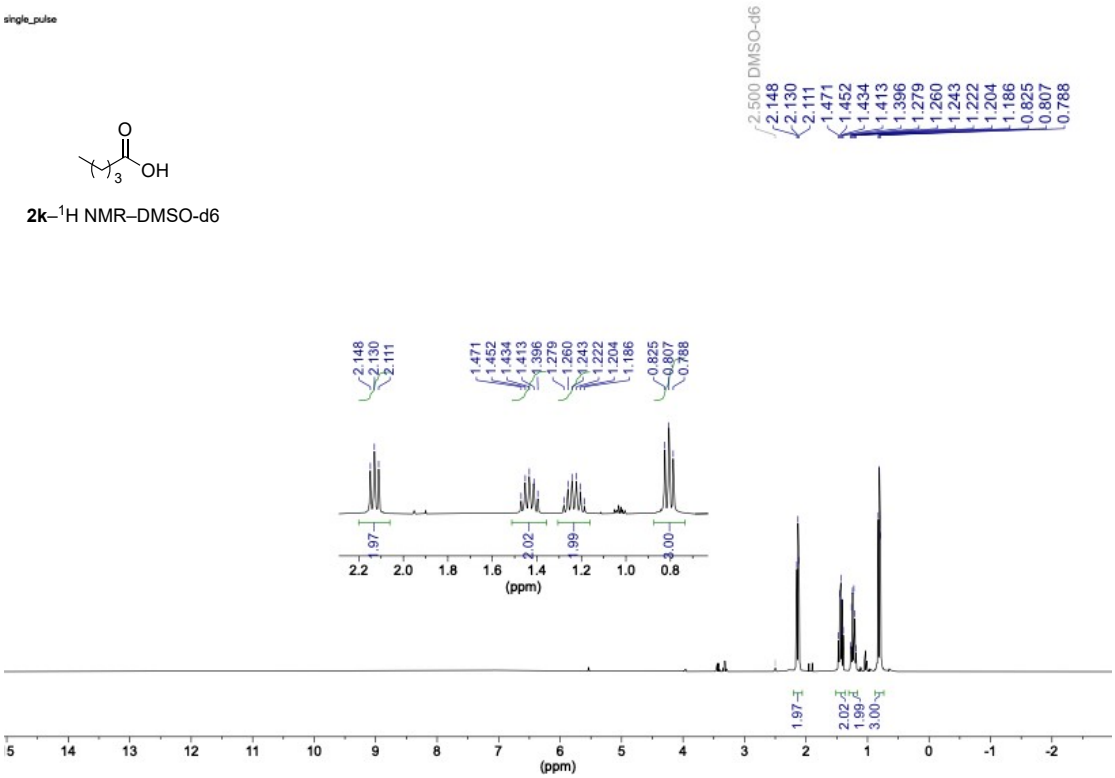

2k–^{1}H NMR–DMSO-d6

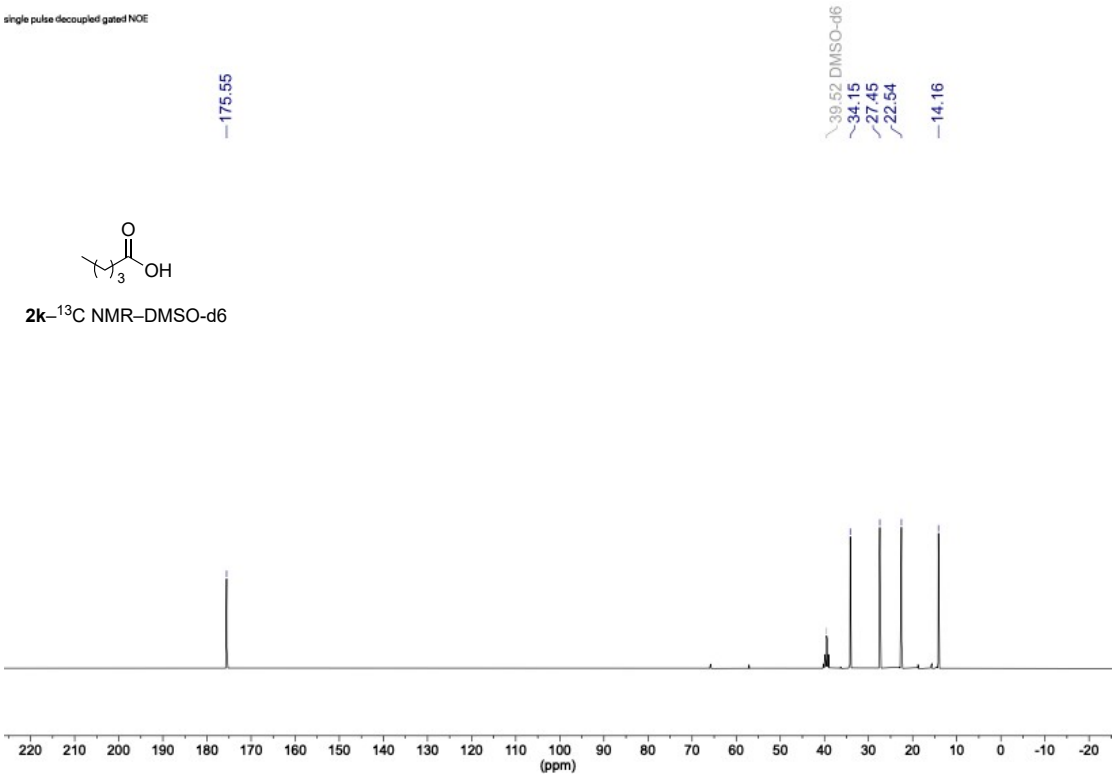

2k–^{13}C NMR–DMSO-d6

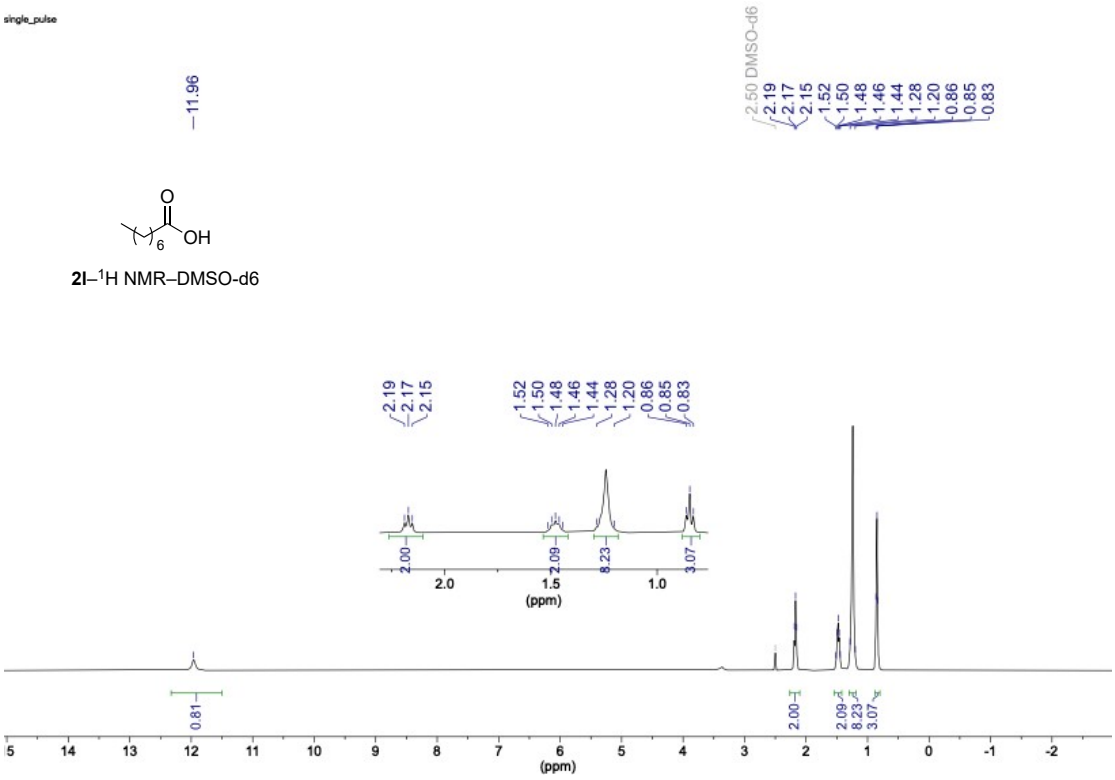

2l–^{1}H NMR–DMSO-d6

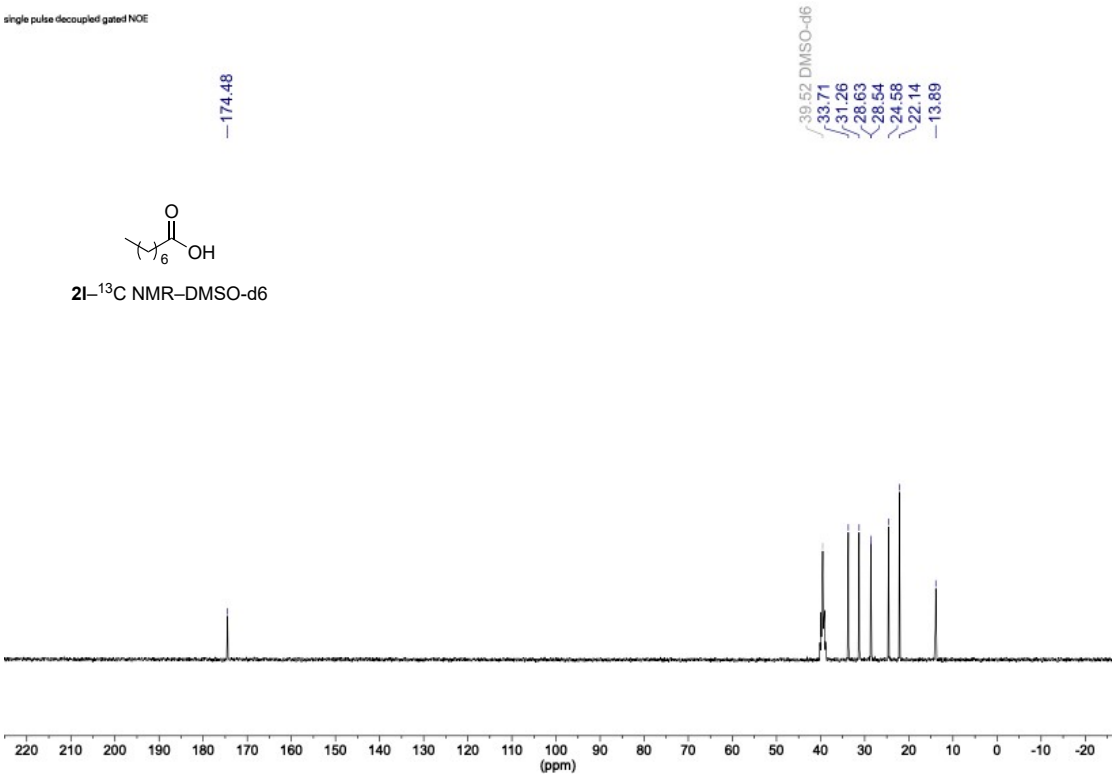

2l–^{13}C NMR–DMSO-d6

2m–^{1}H NMR–DMSO-d6

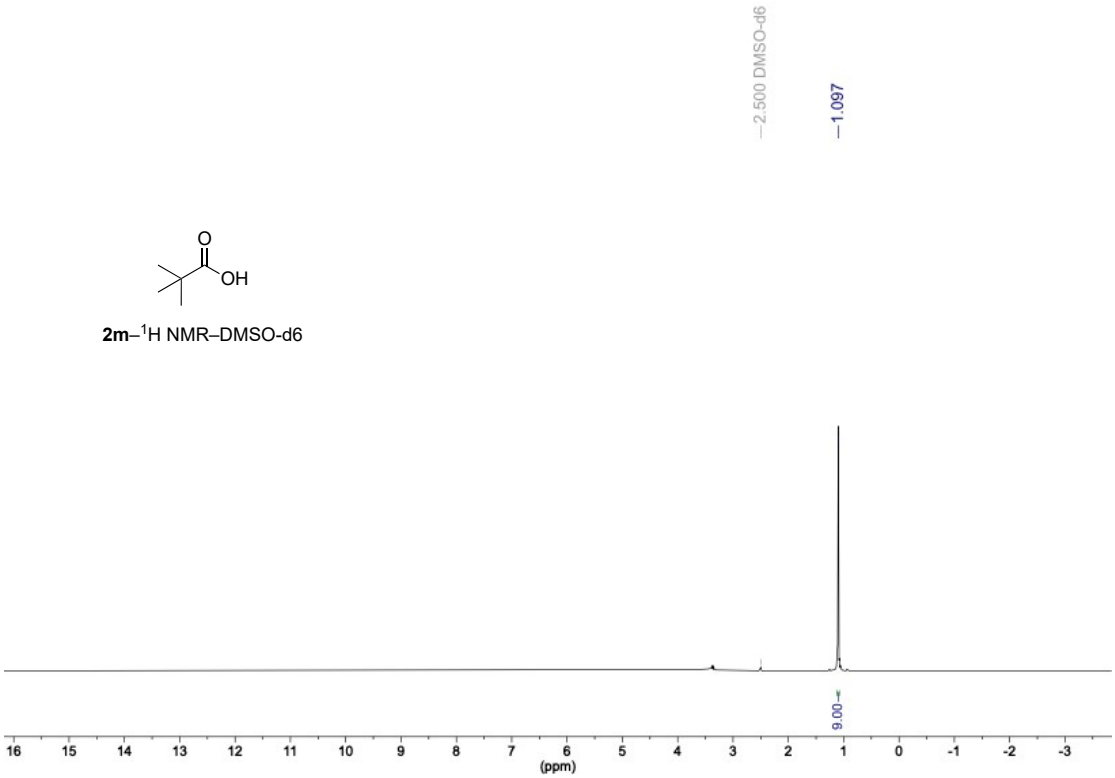

2m–^{13}C NMR–DMSO-d6

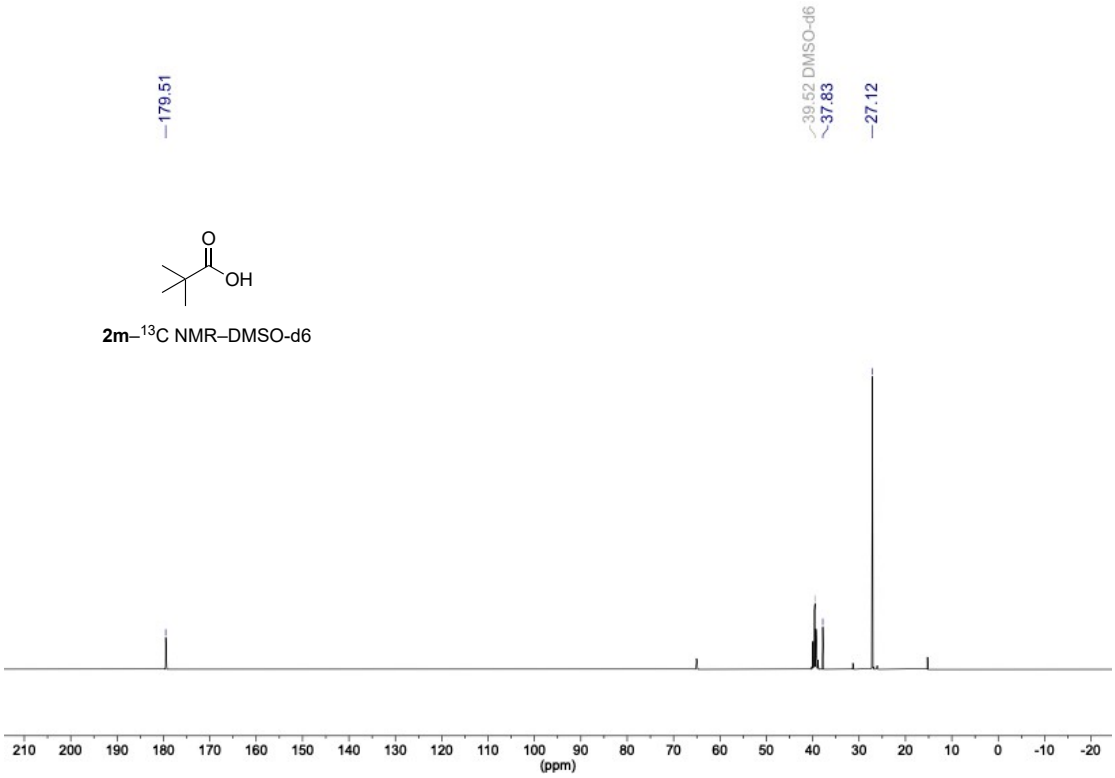

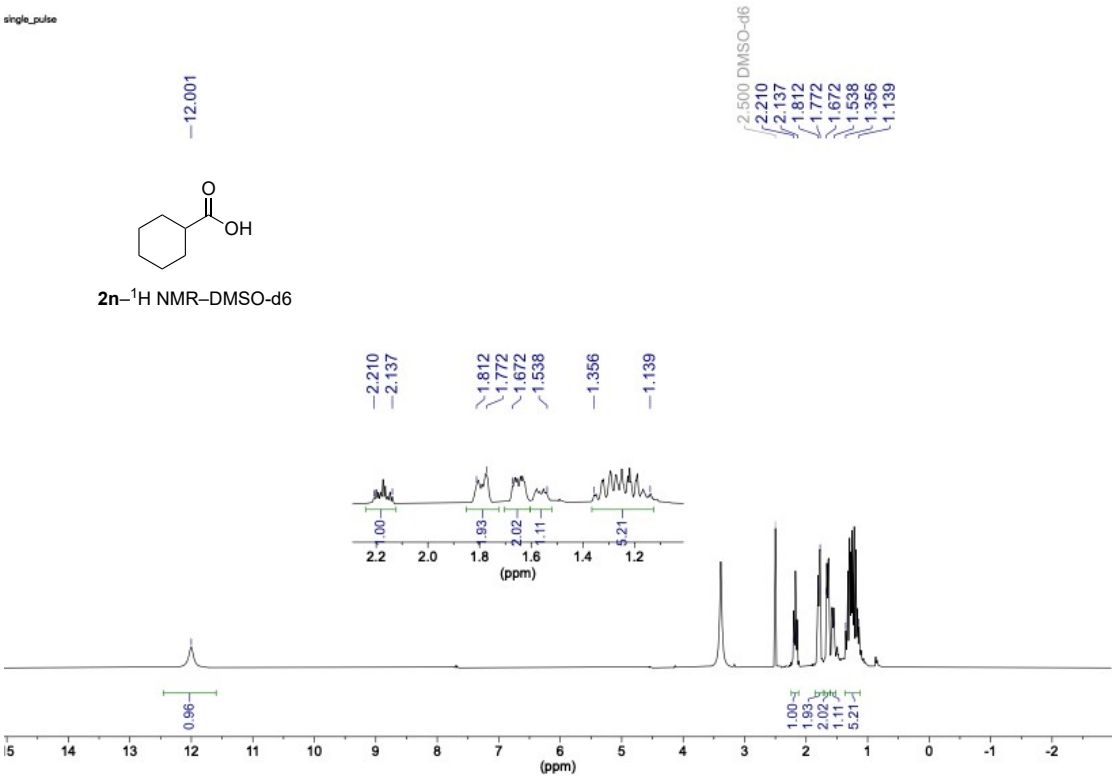

2n–^{1}H NMR–DMSO-d6

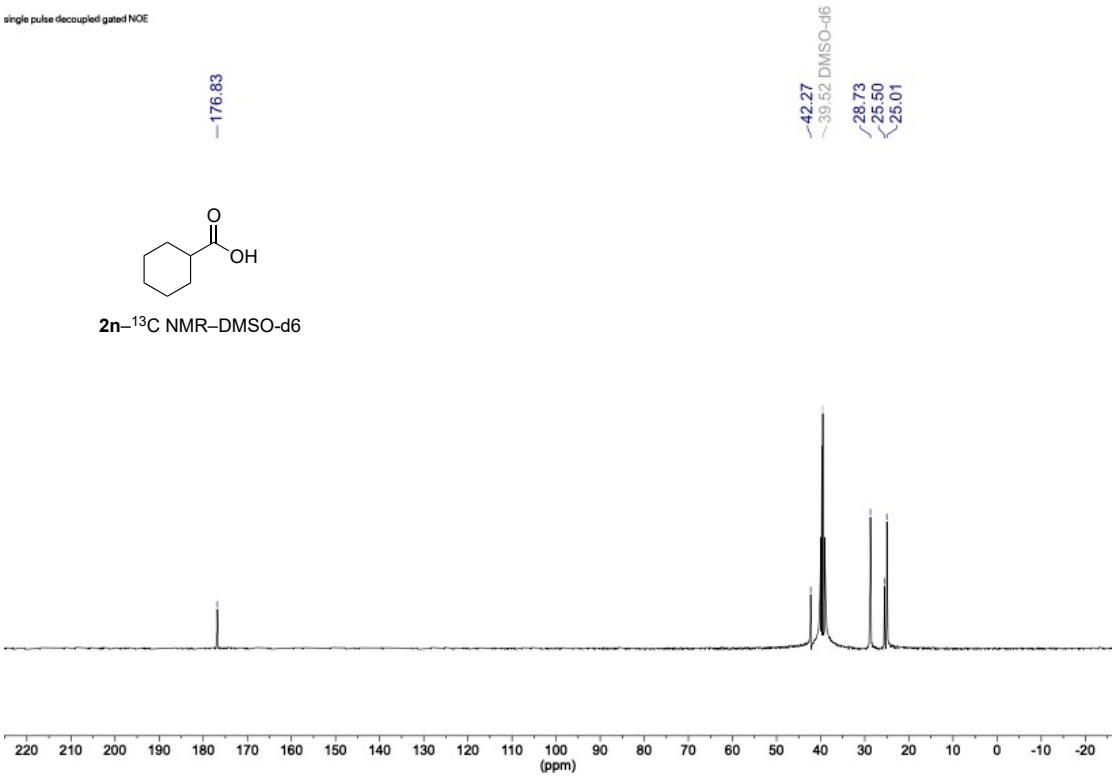

2n–^{13}C NMR–DMSO-d6